Supplementary Information

Synthesis of covalently bounded MWCNT-oligoethylene Linezolid conjugates and their antibacterial activity against bacterial strains

José A. Alatorre-Barajas,[1] Eleazar Alcántar-Zavala,[1] M. Graciela Gil-Rivas,[1] Edgar Estrada-Zavala,[2] Adrián Ochoa-Terán,[1]* Y. Gochi-Ponce,[1]* Julio Montes-Ávila,[2] Alberto Cabrera,[1] Balter Trujillo-Navarrete,[1] Yazmin Yorely Rivera-Lugo,[1] Gabriel Alonso-Núñez,[3] Edgar A. Reynoso-Soto,[1] J. L. Medina-Franco[4]

[1] Centro de Graduados e Investigación en Química. Tecnológico Nacional de México/ IT de Tijuana. Tijuana, B. C. México.

[2] Facultad de Ciencias Químico Biológicas, Universidad Autónoma de Sinaloa. Culiacán, Sin. México.

[3] Centro de Nanociencias y Nanotecnología, Universidad Nacional Autónoma de México. Ensenada, B. C. México.

[4] Departamento de Farmacia, Facultad de Química, Universidad Nacional Autónoma de México, Ciudad de México. México.

*Corresponding email: adrian.ochoa@tectijuana.edu.mx, yadira.gochi@tectijuana.edu.mx

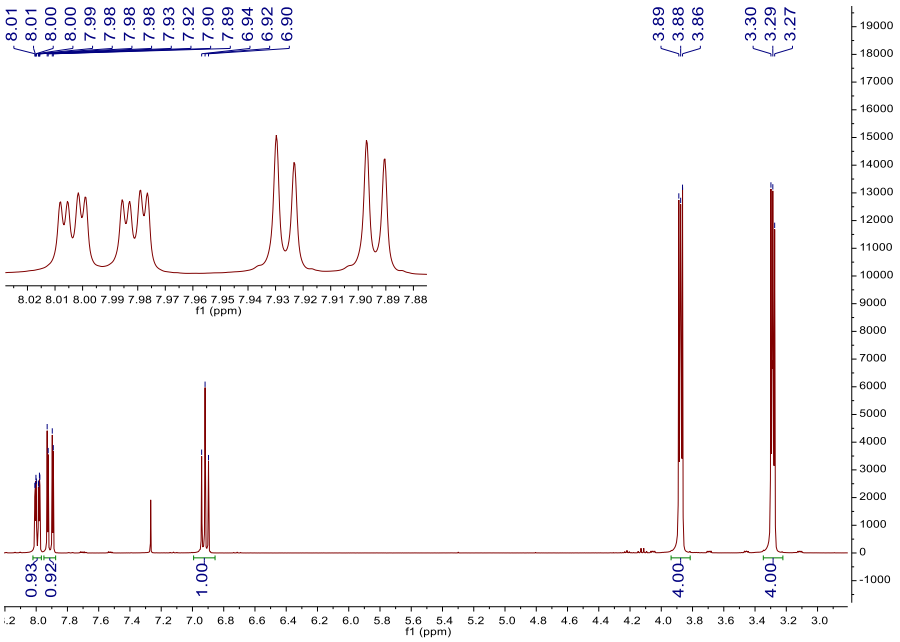

Figure S1. ^{1}H NMR ($CDCl_3$, 400 MHz) of 3-fluoro-4-morpholinylnitrobenzene (**1**).

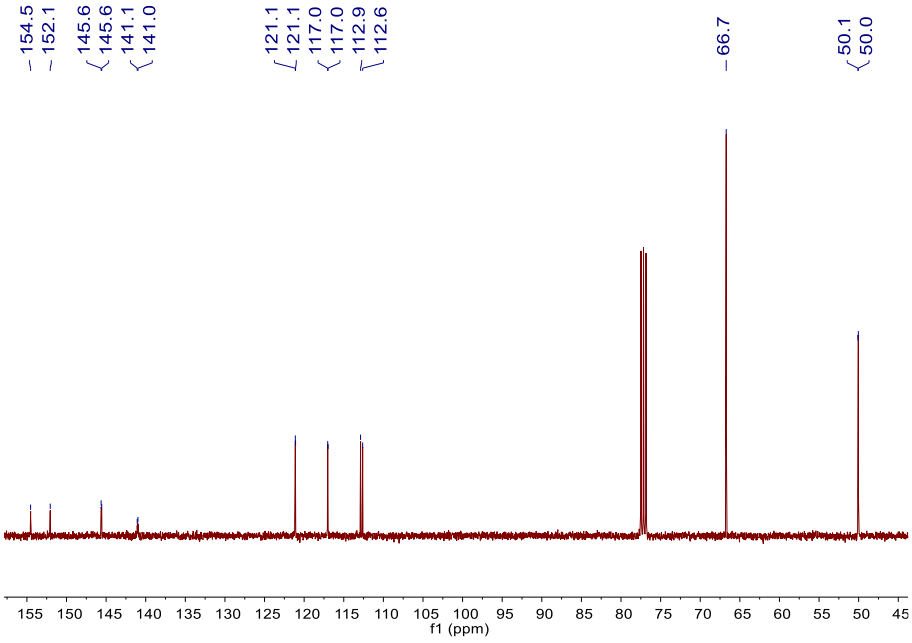

Figure S2. ^{13}C NMR ($CDCl_3$, 400 MHz) of 3-fluoro-4-morpholinylnitrobenzene (**1**).

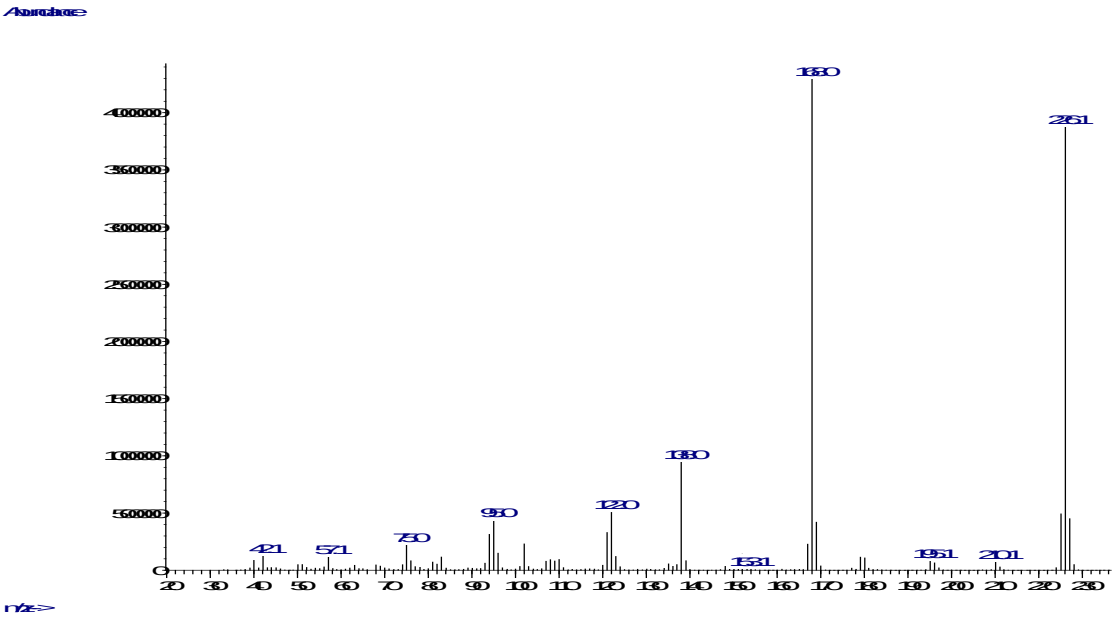

Figure S3. MS(EI) of 3-fluoro-4-morpholinylnitrobenzene (**1**).

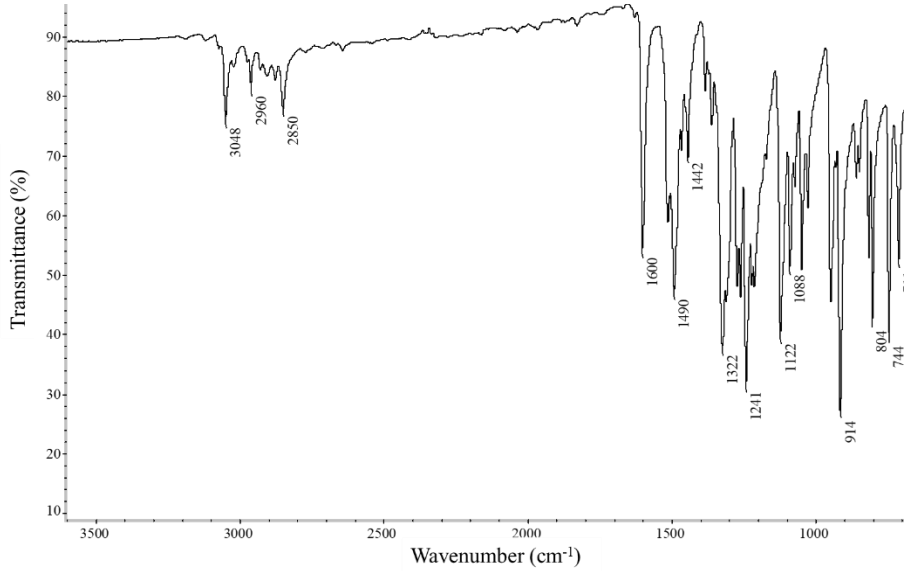

Figure S4. FTIR of 3-fluoro-4-morpholinylnitrobenzene (**1**).

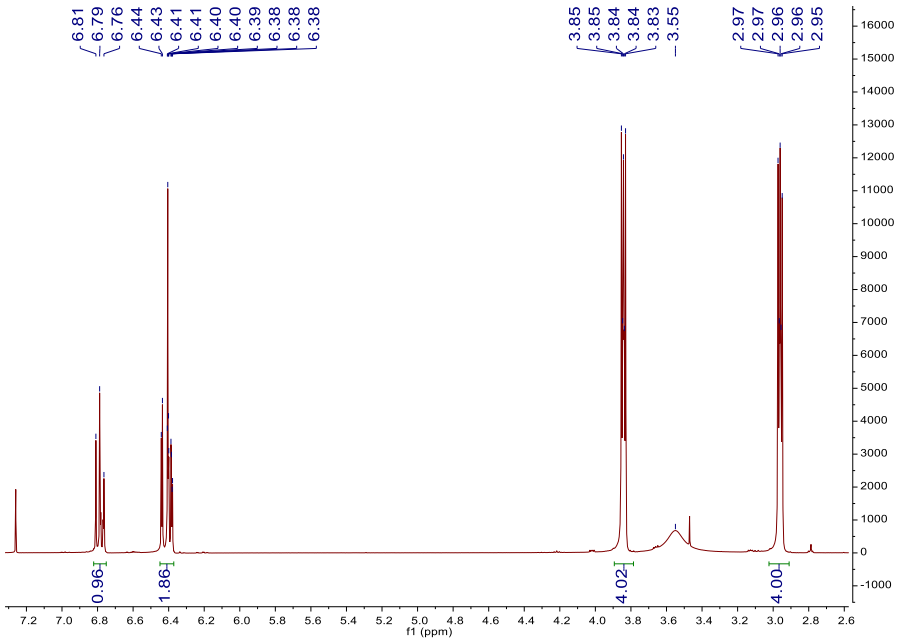

Figure S5. ^{1}H NMR ($CDCl_3$, 400 MHz) of 3-fluoro-4-morpholinylaniline (**2**).

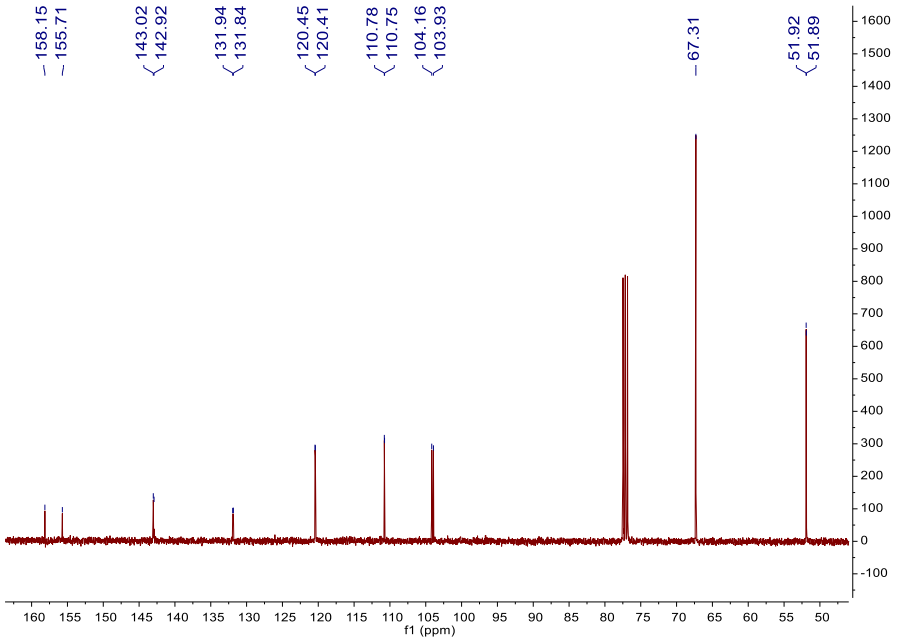

Figure S6. ^{13}C NMR ($CDCl_3$, 400 MHz) of 3-fluoro-4-morpholinylaniline (**2**).

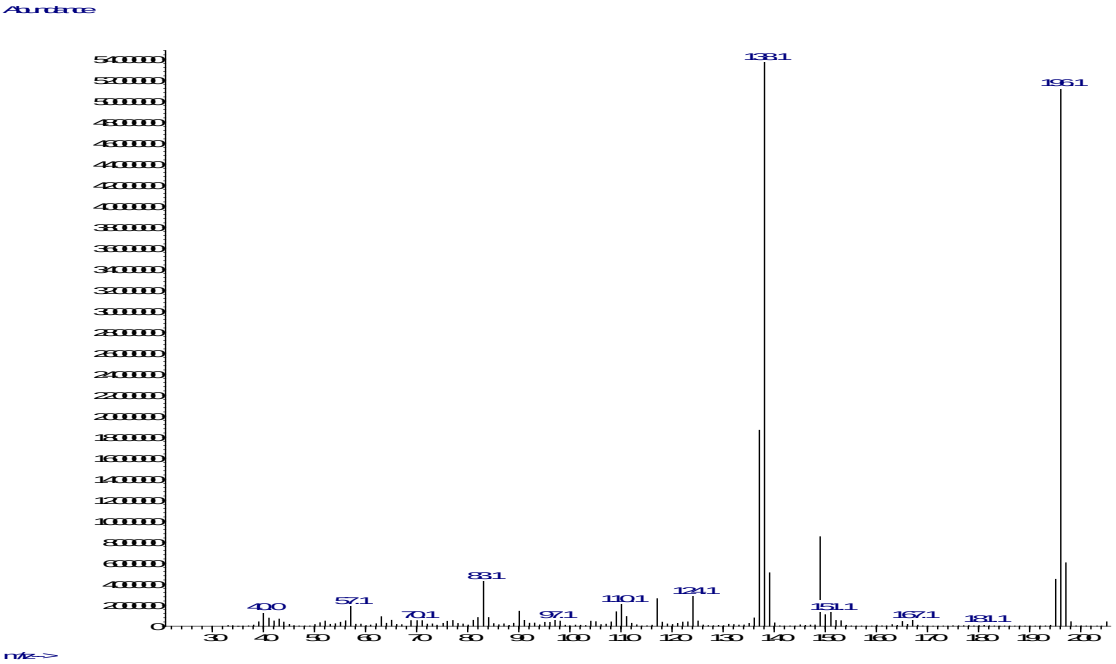

Figure S7. MS(EI) of 3-fluoro-4-morpholinylaniline (**2**).

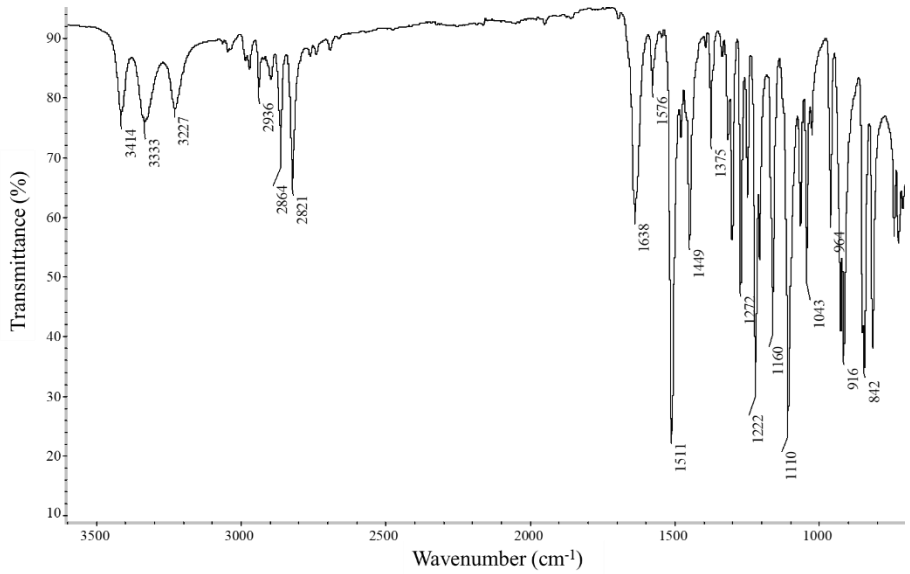

Figure S8. FTIR of 3-fluoro-4-morpholinylaniline (**2**).

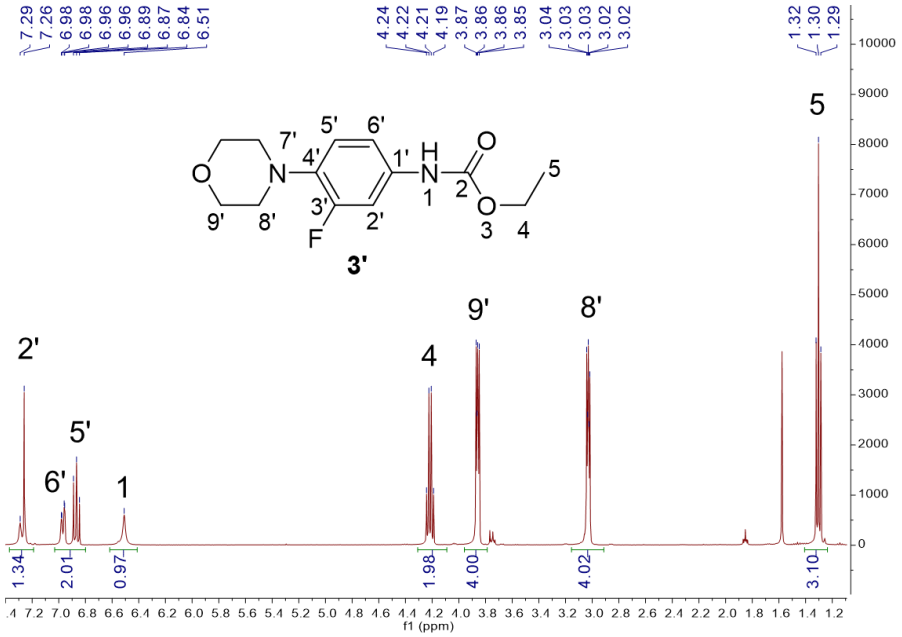

Figure S9. ^{1}H NMR ($CDCl_3$, 400 MHz) of *N*-carboethoxy-3-fluoro-4-morpholinylaniline (**3**).

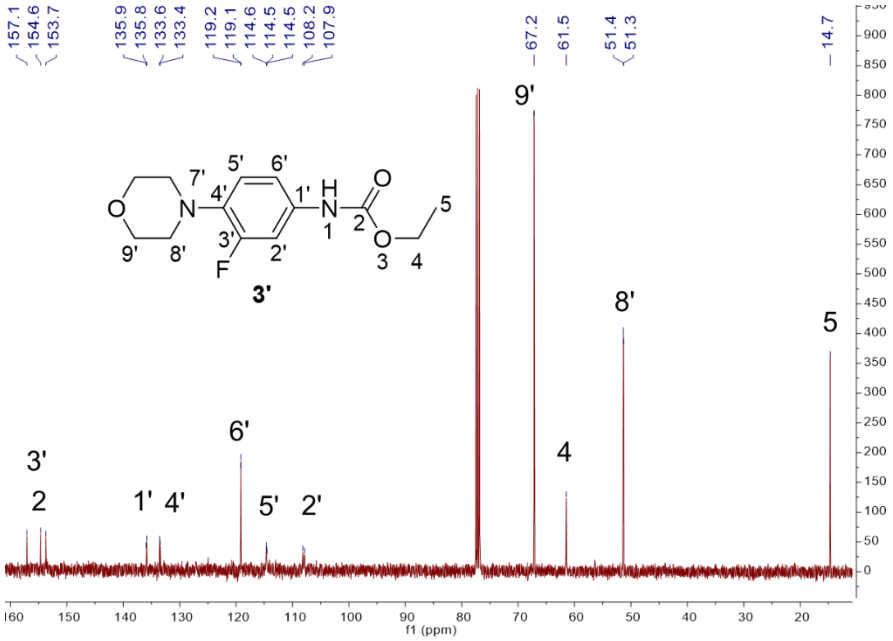

Figure S10. ^{13}C NMR ($CDCl_3$, 400 MHz) of *N*-carboethoxy-3-fluoro-4-morpholinylaniline (**3**).

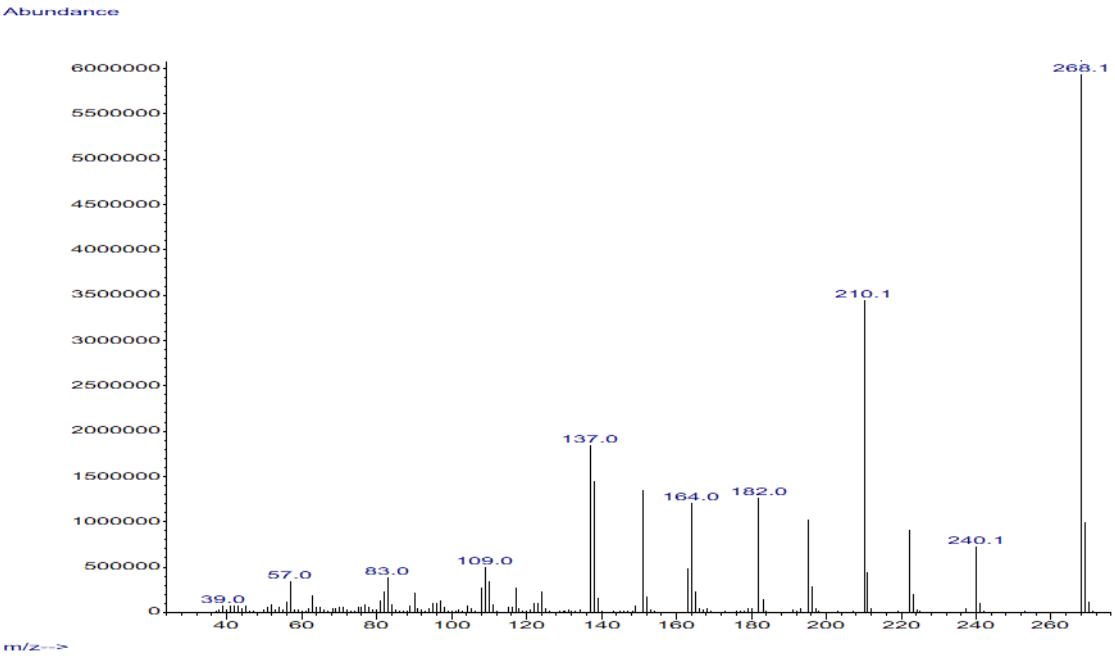

Figure S11.MS(EI) of *N*-carboethoxy-3-fluoro-4-morpholinylaniline (**3**).

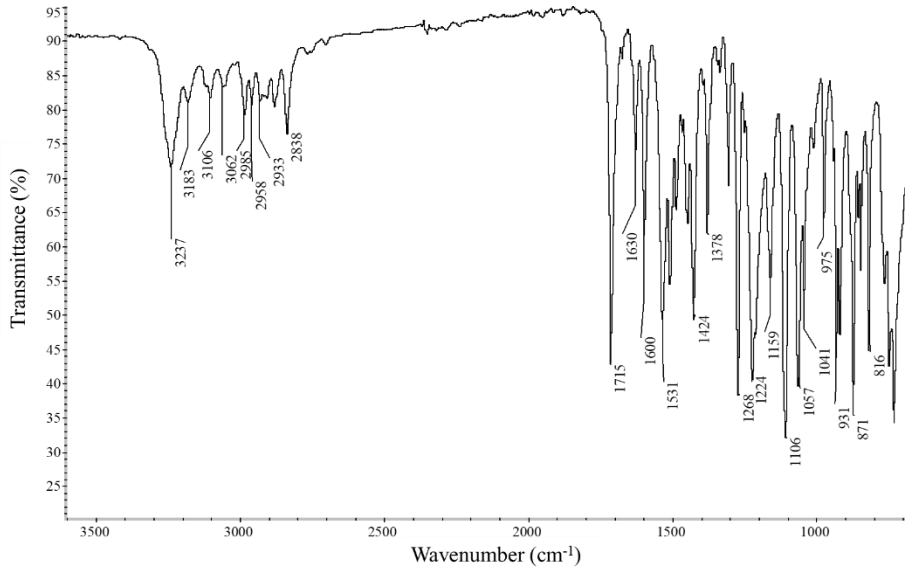

Figure S12. FTIR of *N*-carboethoxy-3-fluoro-4-morpholinylaniline (**3**).

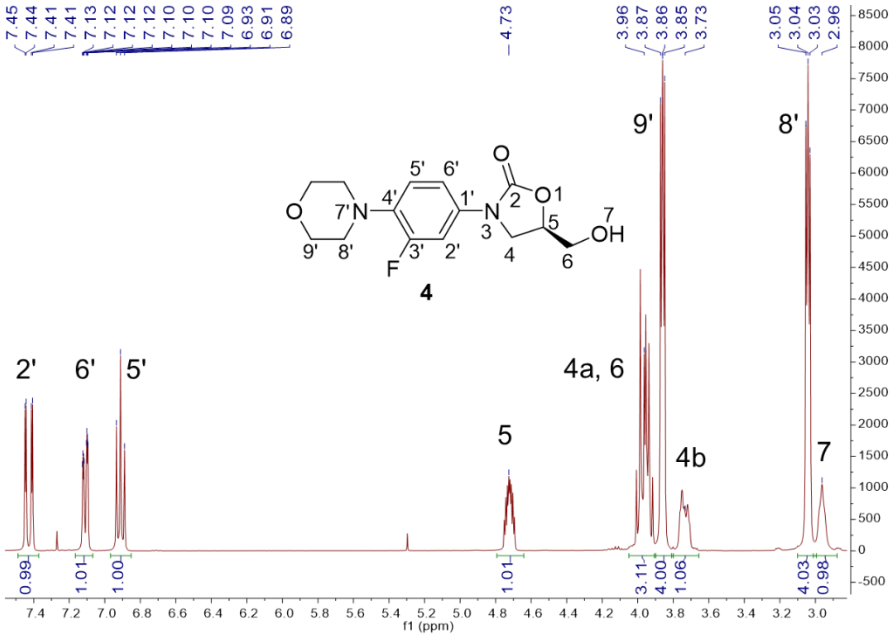

Figure S13. ^{1}H NMR ($CDCl_3$, 400 MHz) of (*R*)-[*N*-3-(3-fluoro-4-morpholinylphenyl)-2-oxo-5-oxazolidinyl]methanol (**4**).

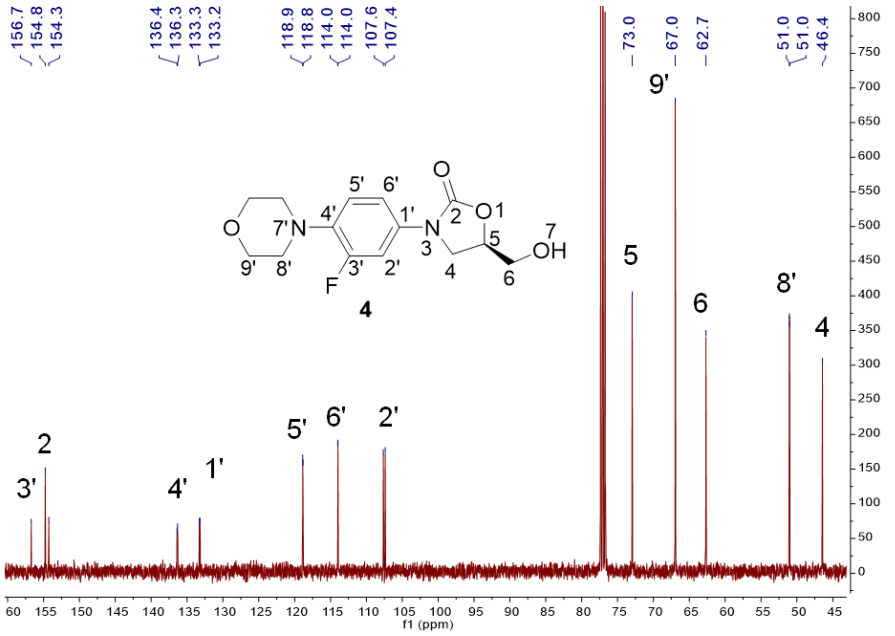

Figure S14. ^{13}C NMR ($CDCl_3$, 400 MHz) of (*R*)-[*N*-3-(3-fluoro-4-morpholinylphenyl)-2-oxo-5-oxazolidinyl]methanol **(4)**.

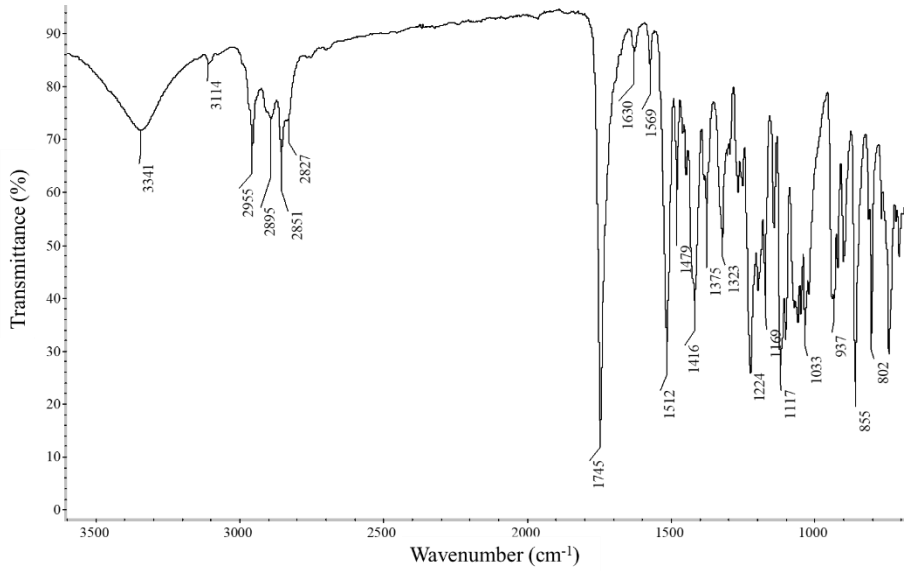

Figure S15. FTIR of (*R*)-[*N*-3-(3-fluoro-4-morpholinylphenyl)-2-oxo-5-oxazolidinyl]methanol (**4**).

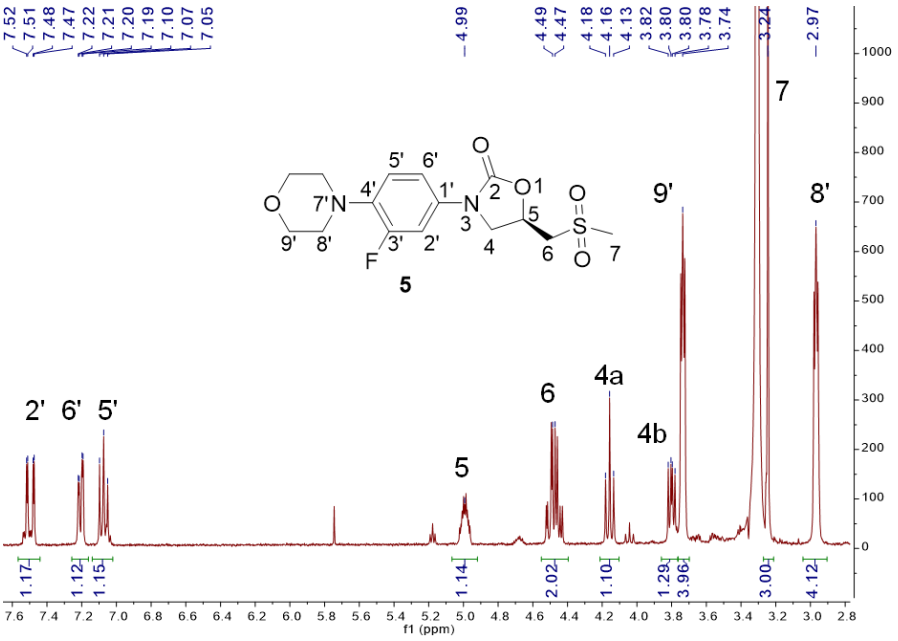

Figure S16. ^{1}H NMR (DMSO-d_6, 400 MHz) of (*R*)-[*N*-3-(3-fluoro-4-morpholinylphenyl)-2-oxo-5-oxazolidinyl]methyl methanesulfonate (**5**).

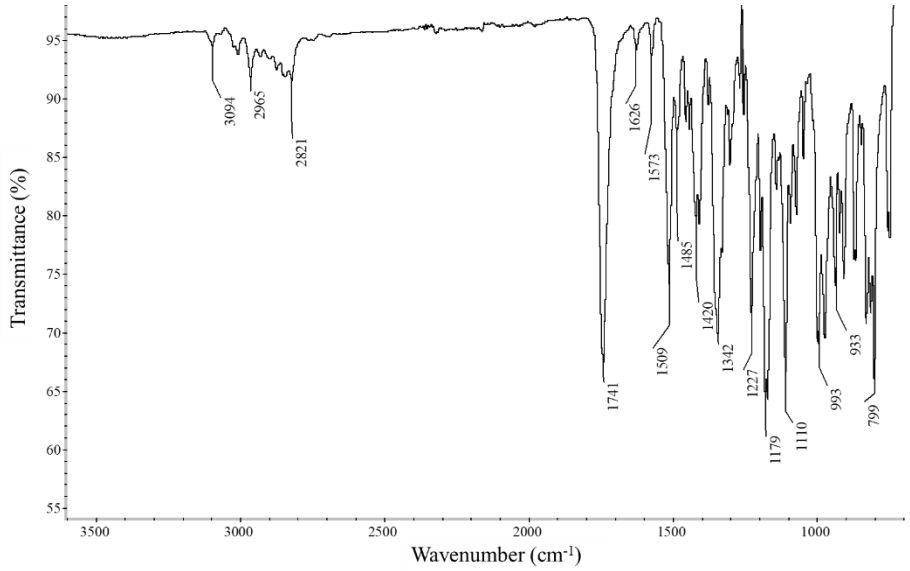

Figure S17. FTIR of (*R*)-[*N*-3-(3-fluoro-4-morpholinylphenyl)-2-oxo-5-oxazolidinyl]methyl methanesulfonate (**5**).

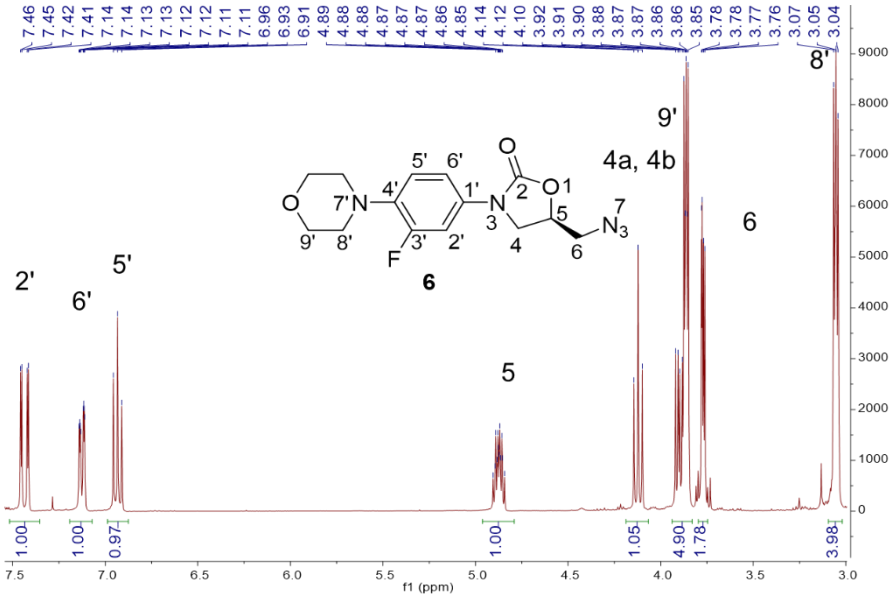

Figure S18. ^{1}H NMR ($CDCl_3$, 400 MHz) of (*R*)-[*N*-3-(3-fluoro-4-morpholinylphenyl)-2-oxo-5-oxazolidinyl]methyl azide (**6**).

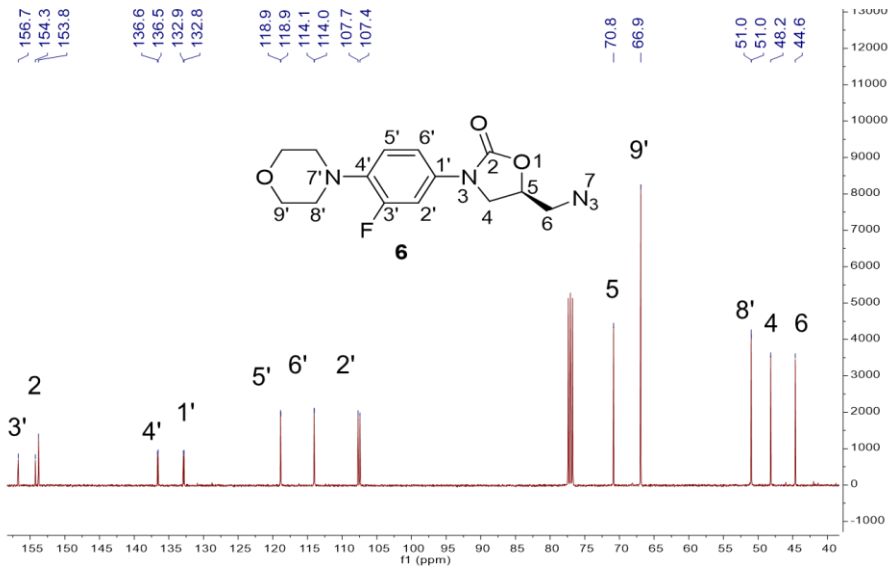

Figure S19. ^{13}C NMR ($CDCl_3$, 400 MHz) of (*R*)-[*N*-3-(3-Fluoro-4-morpholinylphenyl)-2-oxo-5-oxazolidinyl]methyl azide (**6**).

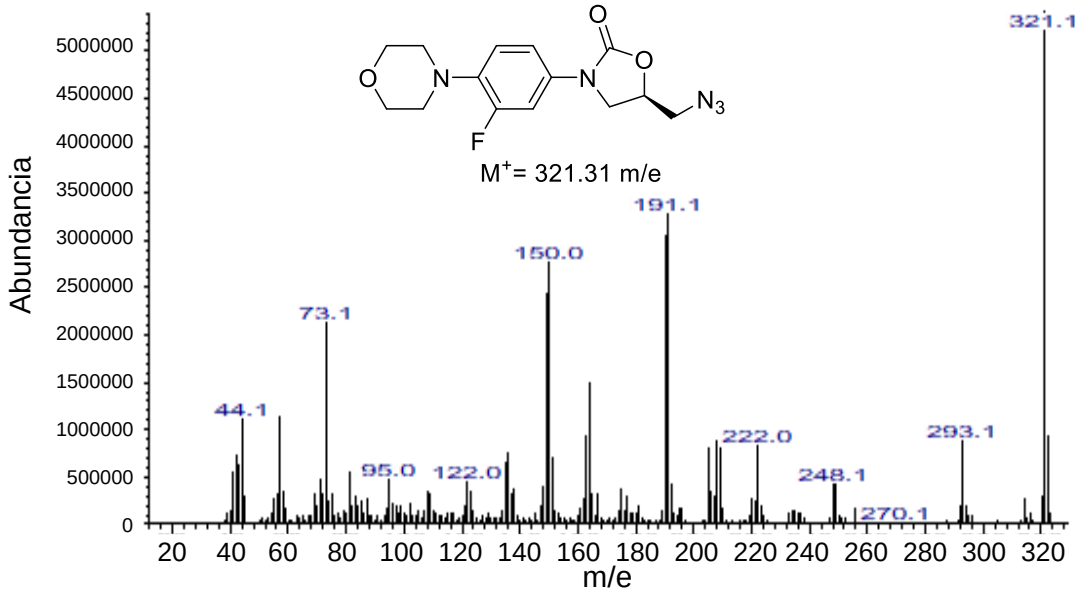

Figure S20. MS(EI) of (*R*)-[*N*-3-(3-fluoro-4-morpholinylphenyl)-2-oxo-5-oxazolidinyl] methyl azide (**6**).

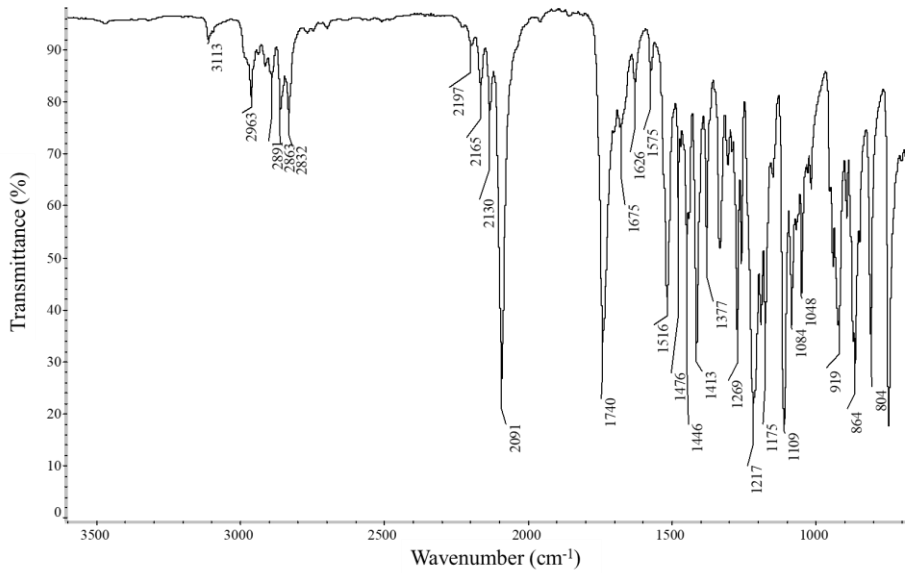

Figure S21. FTIR of (*R*)-[*N*-3-(3-fluoro-4-morpholinylphenyl)-2-oxo-5-oxazolidinyl] methyl azide (**6**).

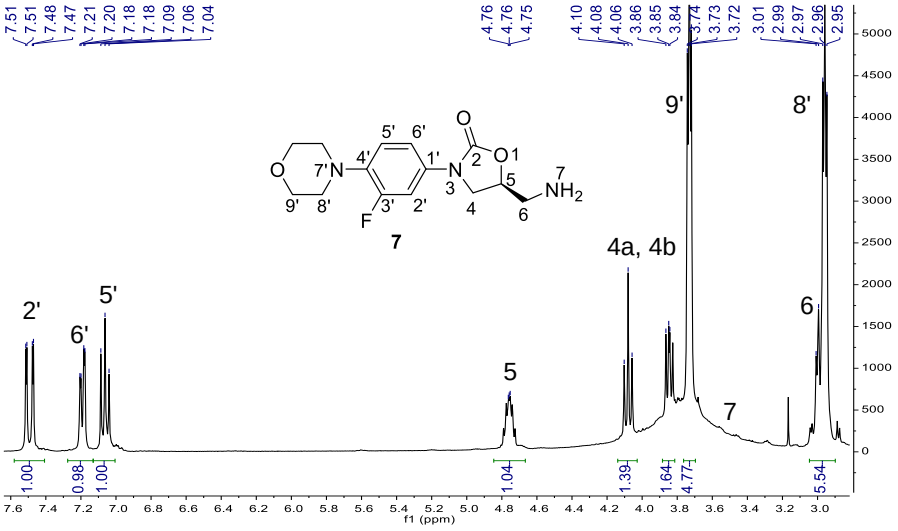

Figure S22. ^{1}H NMR ($CDCl_3$, 400 MHz) of (*R*)-[*N*-3-(3-fluoro-4-morpholinylphenyl)-2-oxo-5-oxazolidinyl]methanamine (**7**).

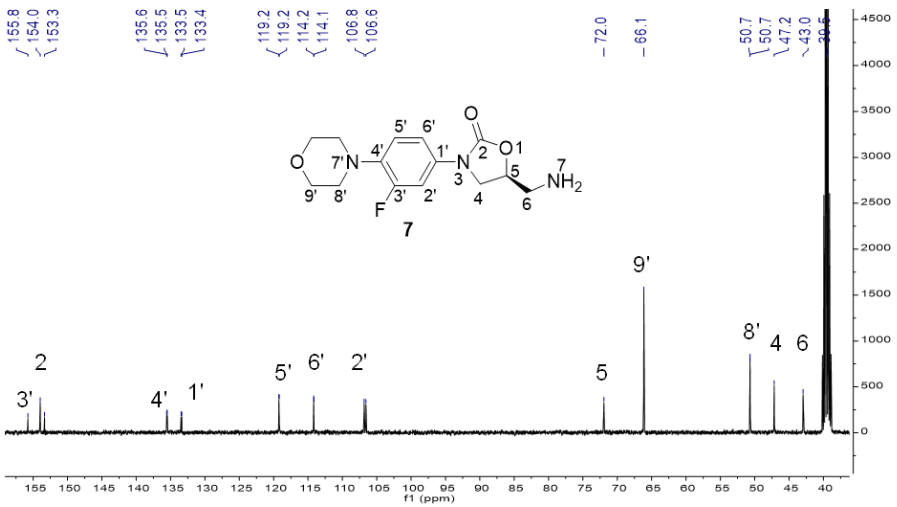

Figure S23. ^{13}C NMR ($CDCl_3$, 400 MHz) of (*R*)-[*N*-3-(3-fluoro-4-morpholinylphenyl)-2-oxo-5-oxazolidinyl]methanamine (**7**).

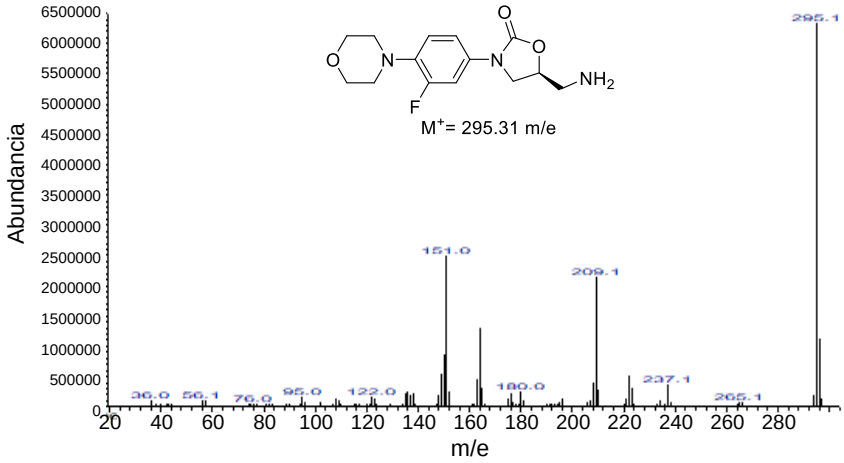

Figure S24. MS(EI) of (*R*)-[*N*-3-(3-fluoro-4-morpholinylphenyl)-2-oxo-5-oxazolidinyl] methanamine (**7**).

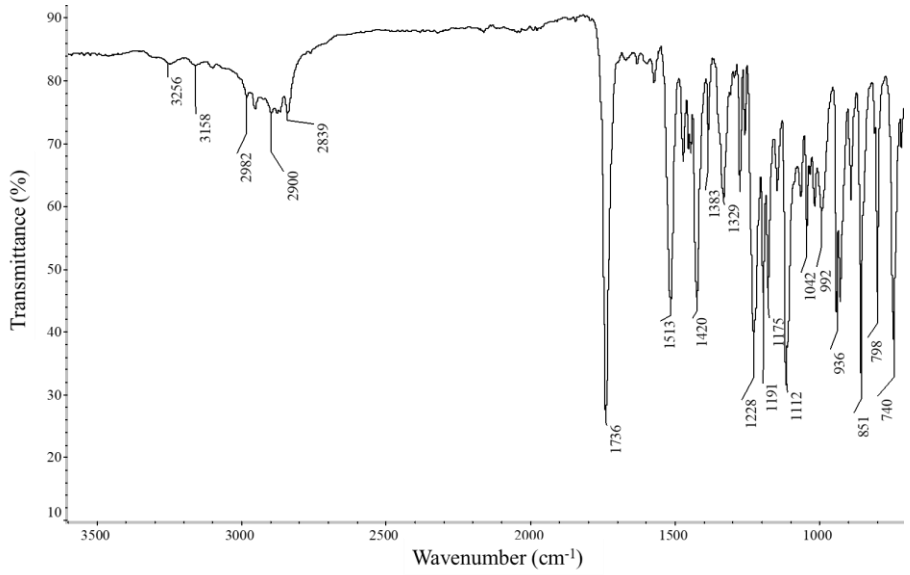

Figure S25. FTIR of (*R*)-[*N*-3-(3-fluoro-4-morpholinylphenyl)-2-oxo-5-oxazolidinyl] methanamine (**7**).

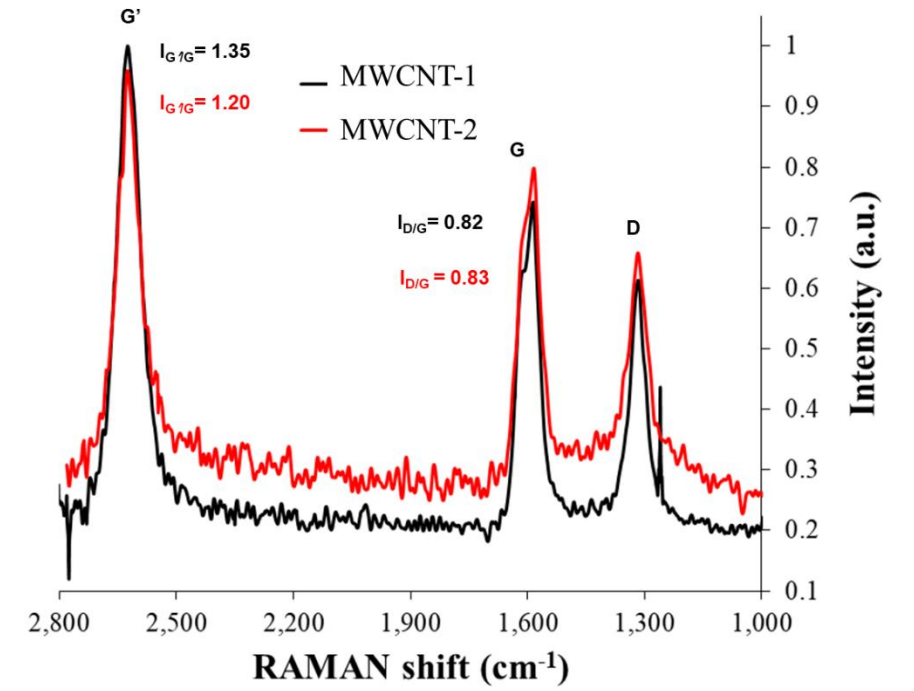

Figure S26. Raman spectra of **MWCNT-1** (black) and **MWCNT-2** (red).

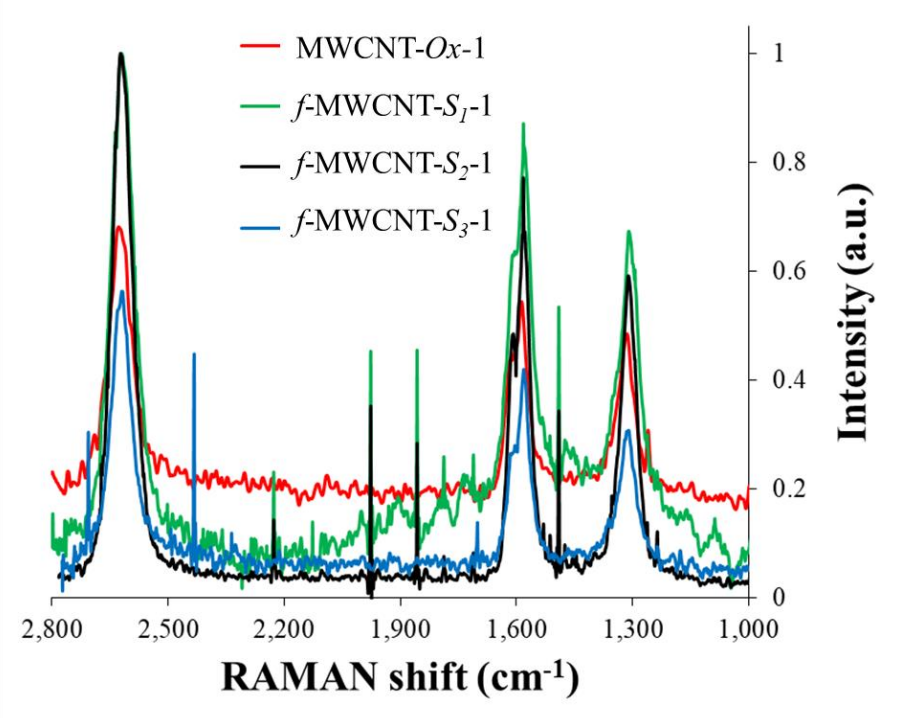

Figure S27. Raman spectra of **MWCNT-*Ox*-1** (red), ***f*-MWCNT-S_1-1** (green)**, *f*-MWCNT-S_2-1** (black) and ***f*-MWCNT-S_3-1** (blue).

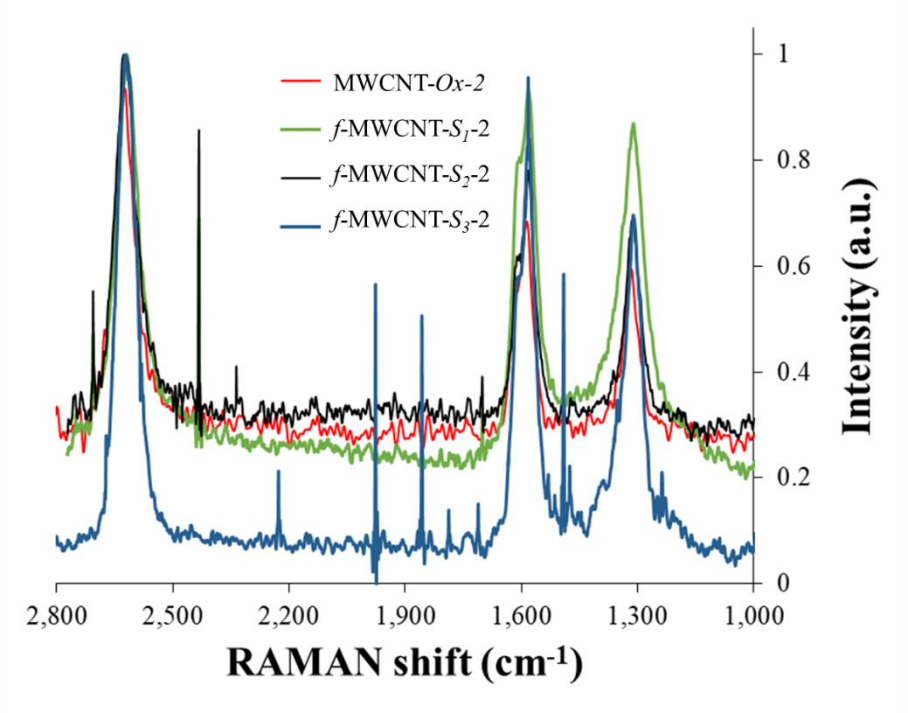

Figure S28. Raman spectra of **MWCNT-*Ox*-2** (red), ***f*-MWCNT-*S*$_1$-2** (green)**, *f*-MWCNT-*S*$_2$-2** (black) and ***f*-MWCNT-*S*$_3$-2** (blue).

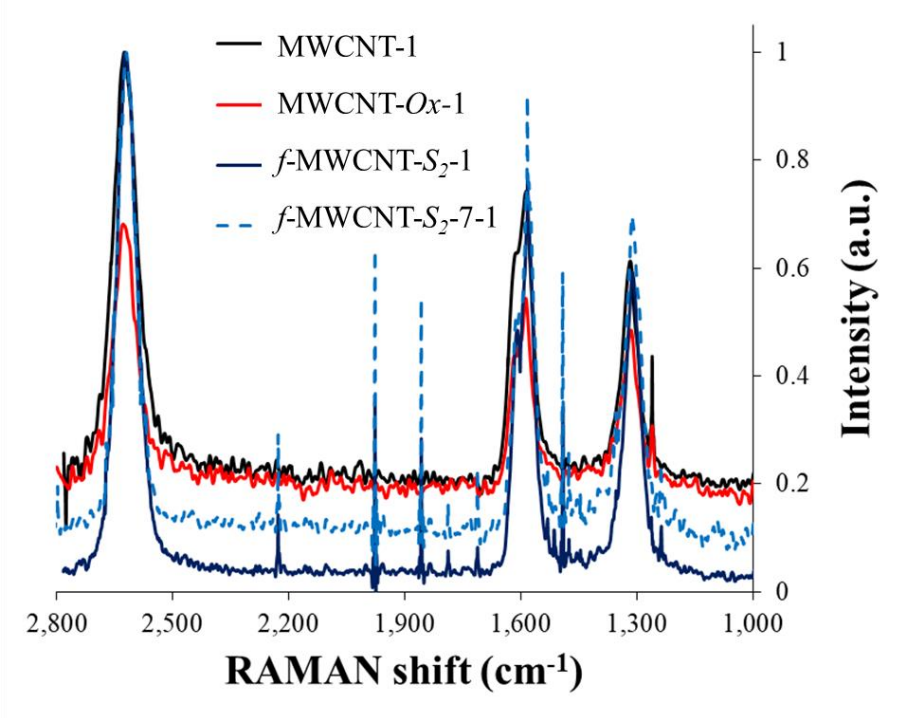

Figure S29. Raman spectra of **MWCNT-1** (black), **MWCNT-*Ox*-1** (red)**, *f*-MWCNT-*S*$_2$-1** (blue solid) and ***f*-MWCNT-*S*$_2$-7-1** (blue dashed).

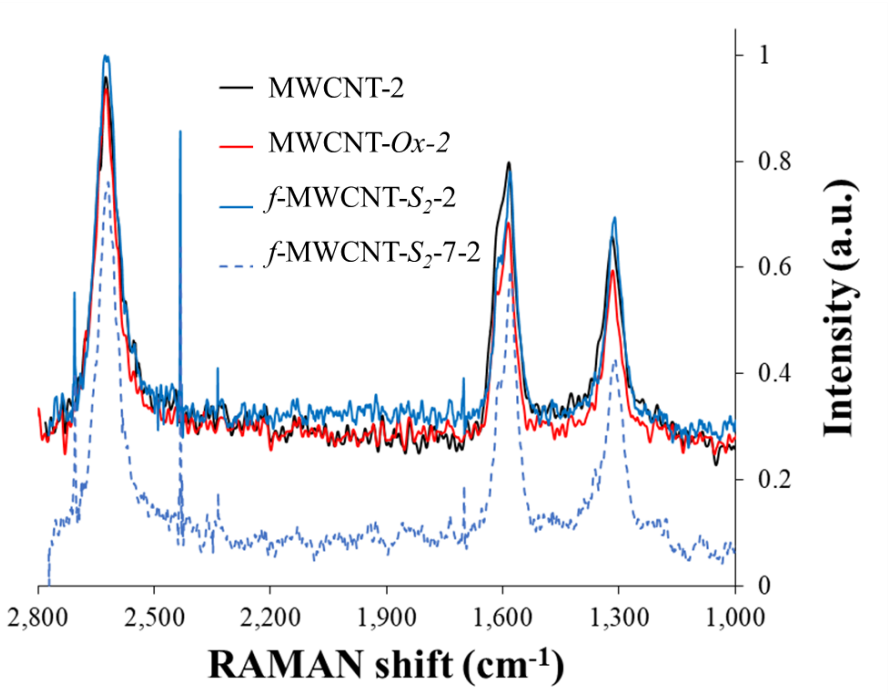

Figure S30. Raman spectra of **MWCNT-2** (black), **MWCNT-*Ox*-2** (red)**, *f*-MWCNT-S_2-2** (blue solid) and ***f*-MWCNT-S_3-2** (blue dashed).

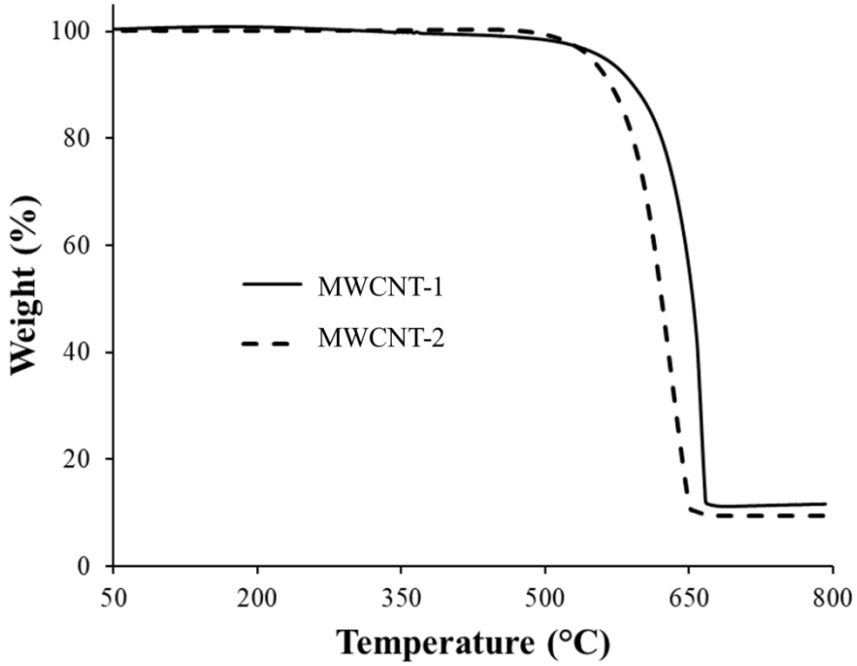

Figure S31. Thermograms of **MWCNT-1** (solid line) and **MWCNT-2** (dashed line).

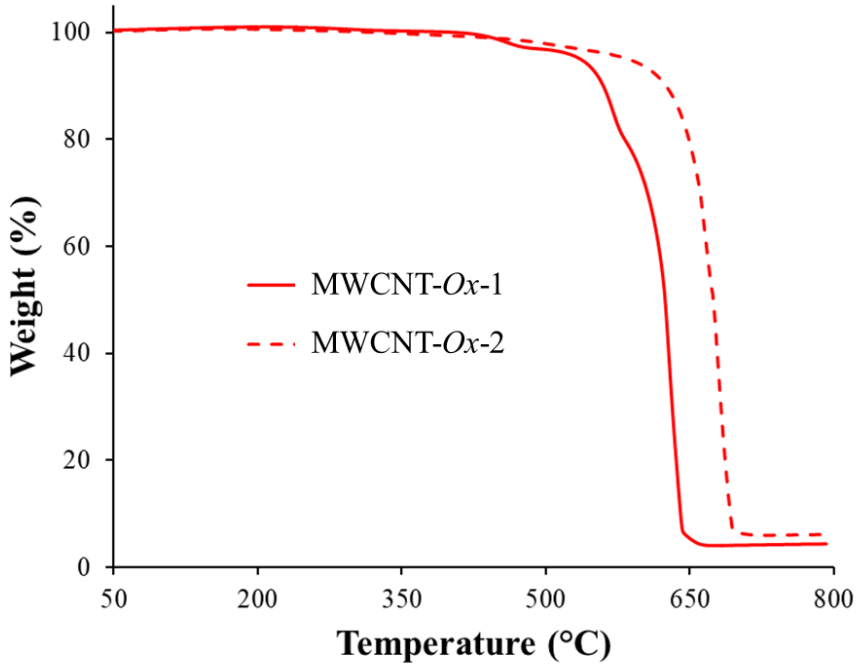

Figure S32. Thermograms of **MWCNT-*Ox*-1** (solid line) and **MWCNT-*Ox*-2** (dashed line).

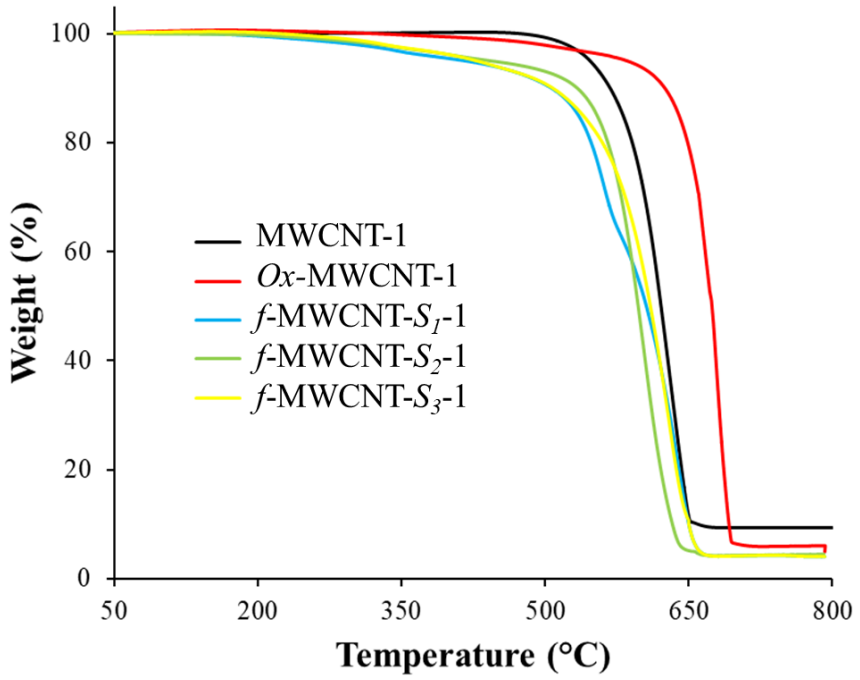

Figure S33. Thermograms of **MWCNT-1** (black), **MWCNT-*Ox*-1** (red), ***f*-MWCNT-*S*$_1$-1** (blue)**,** ***f*-MWCNT-*S*$_2$-1** (green) and ***f*-MWCNT-*S*$_3$-1** (yellow)**.**

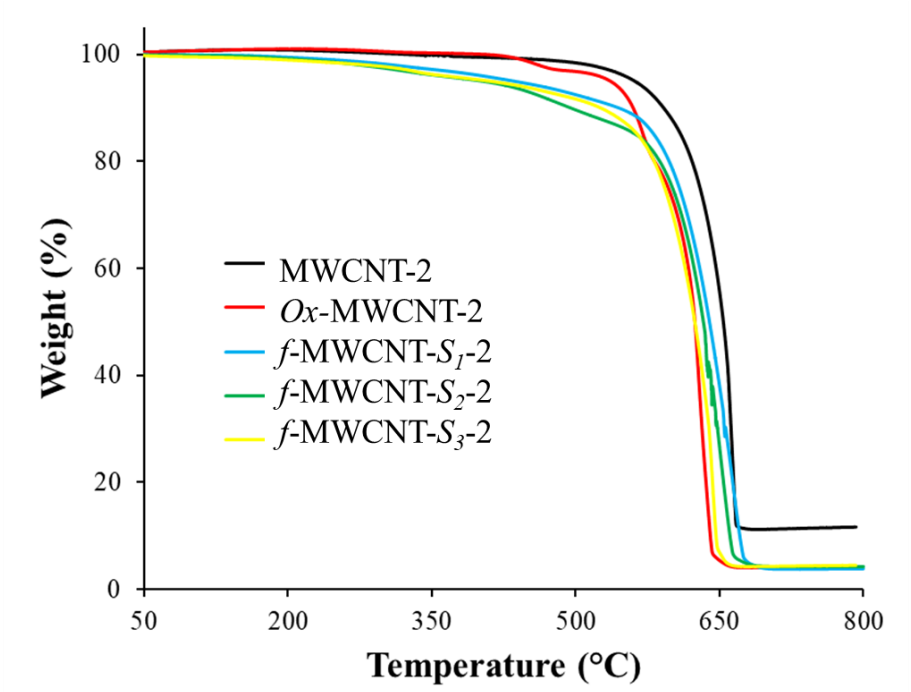

Figure S34. Thermograms of **MWCNT-1** (black), **MWCNT-*Ox*-1** (red), ***f*-MWCNT-*S*$_1$-1** (blue)**, *f*-MWCNT-*S*$_2$-1** (green) and ***f*-MWCNT-*S*$_3$-1** (yellow)**.**

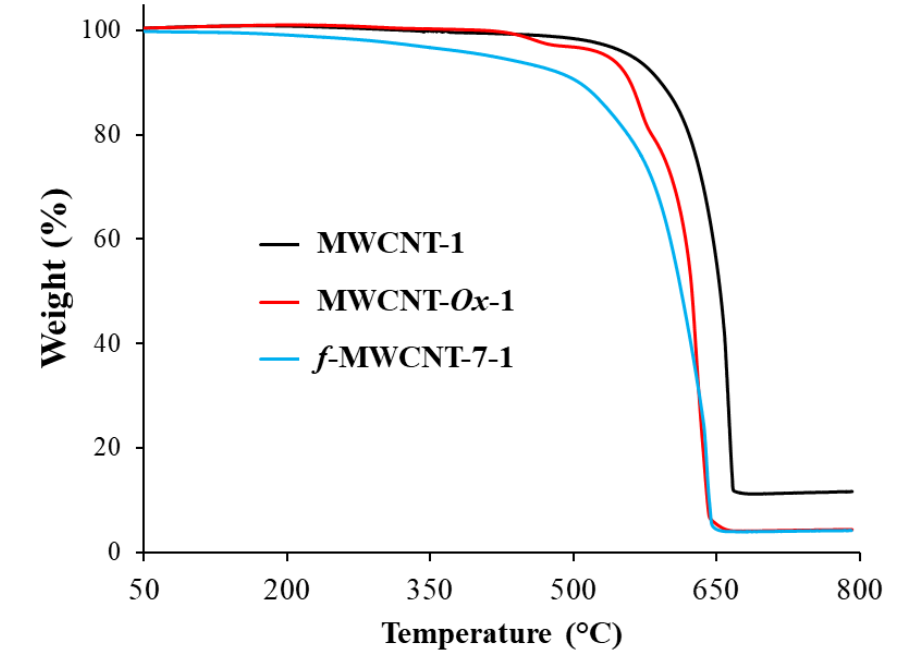

Figure S35. Thermograms of **MWCNT-1** (black), **MWCNT-*Ox*-1** (red) and ***f*-MWCNT-7-1** (blue)**.**

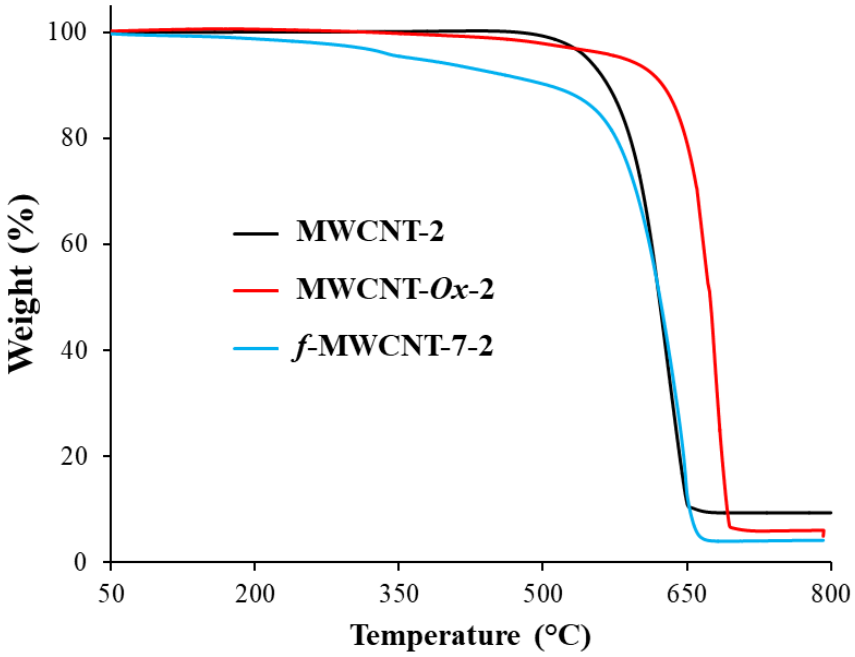

Figure S36. Thermograms of **MWCNT-2** (black), **MWCNT-*Ox*-2** (red) and ***f*-MWCNT-7-2** (blue)**.**

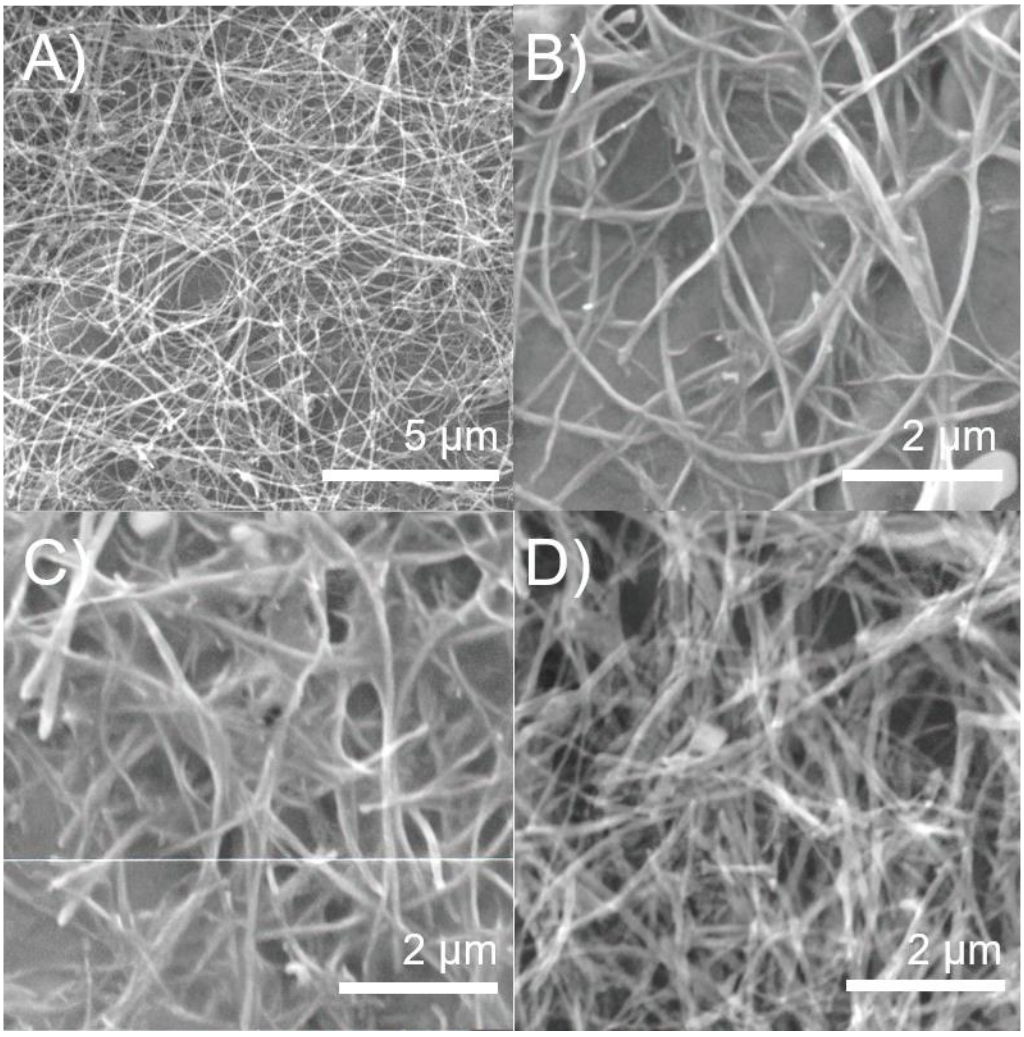

Figure S37. SEM micrographs of A) **MWCNT-2**, B) **MWCNT-*Ox*-2**, C) ***f*-MWCNT-*S*$_1$-1** y D) ***f*-MWCNT-*S*$_1$-7-1**.

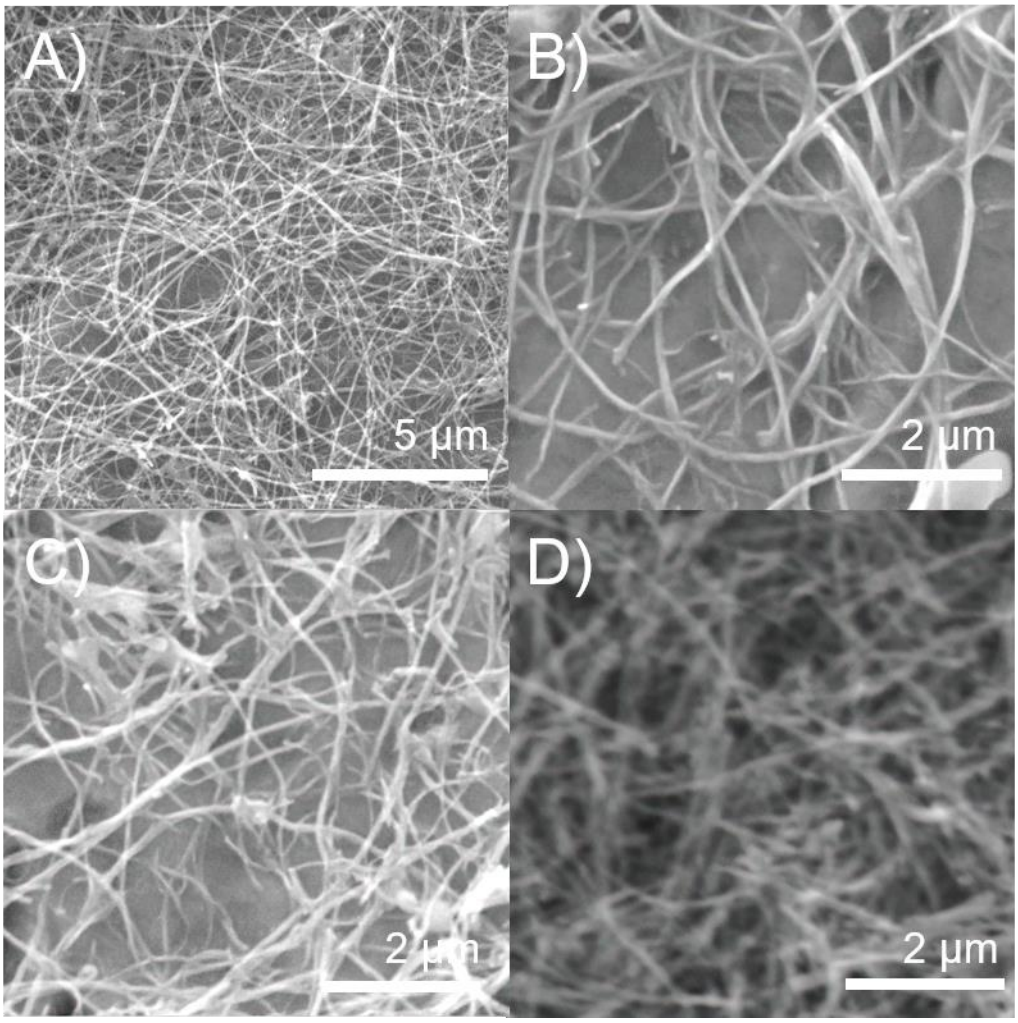

Figure S38. SEM micrographs of A) **MWCNT-1**, B) **MWCNT-*Ox*-1**, C) ***f*-MWCNT-*S*$_2$-1** y D) ***f*-MWCNT-*S*$_2$-7-1**.

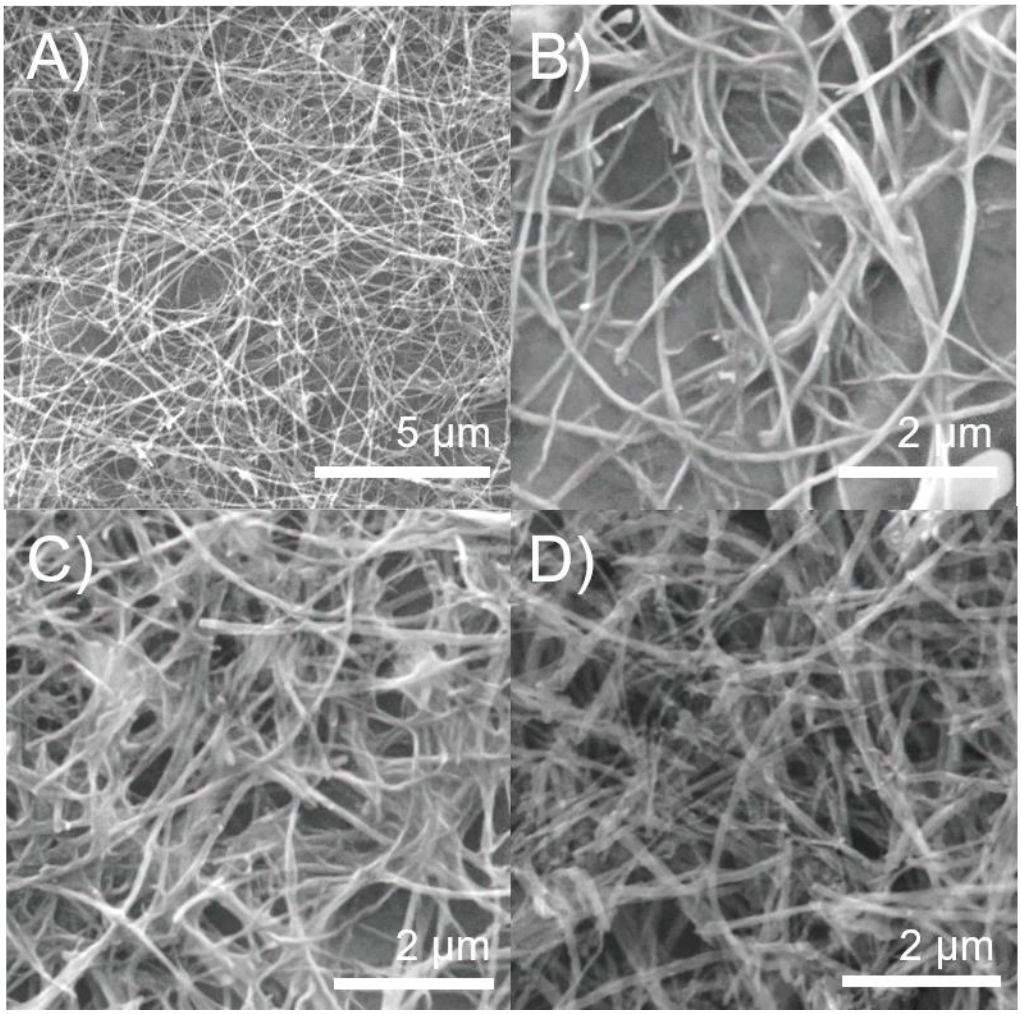

Figure S39. SEM micrographs of A) **MWCNT-1**, B) **MWCNT-*Ox*-1**, C) ***f*-MWCNT-*S*$_3$-1** y D) ***f*-MWCNT-*S*$_3$-7-1**.

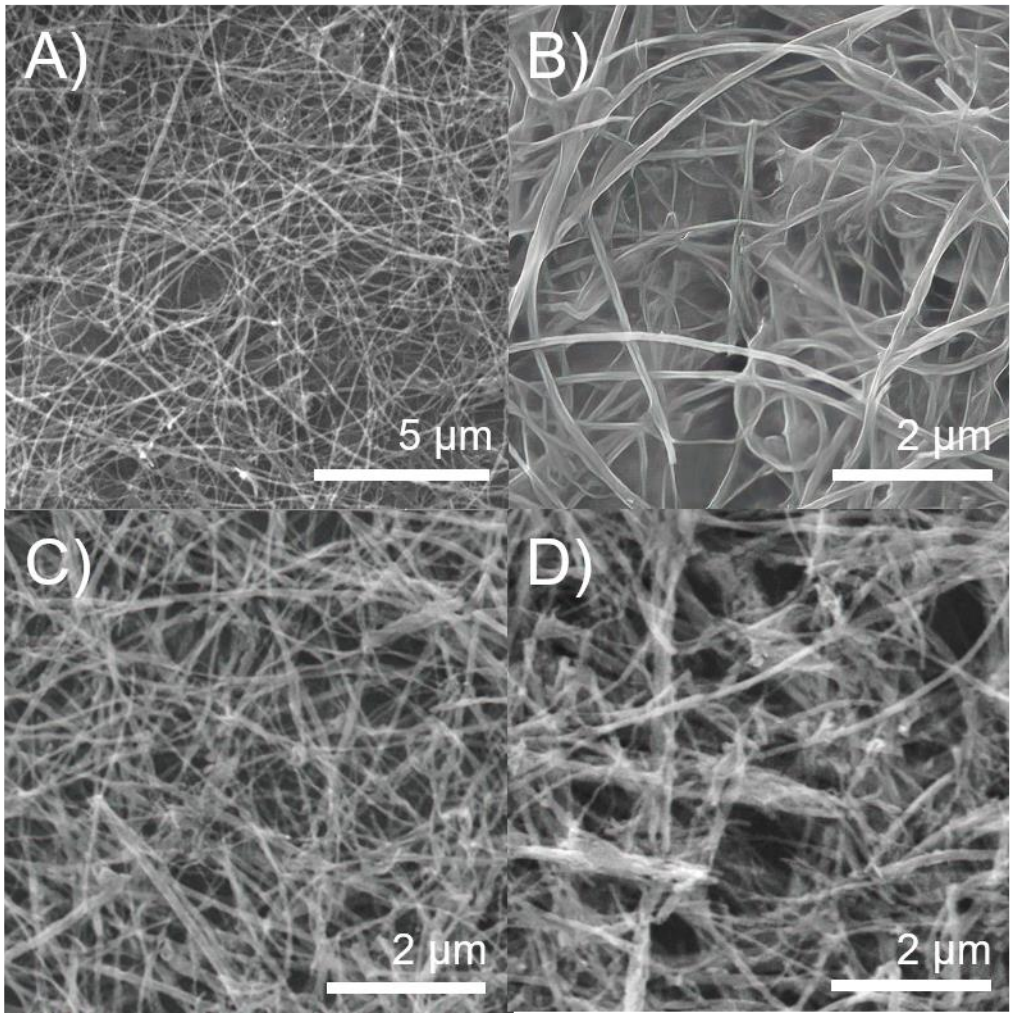

Figure S40. SEM micrographs of A) **MWCNT-2**, B) **MWCNT-*Ox*-2**, C) ***f*-MWCNT-*S*$_1$-2** y D) ***f*-MWCNT-*S*$_1$-7-2**.

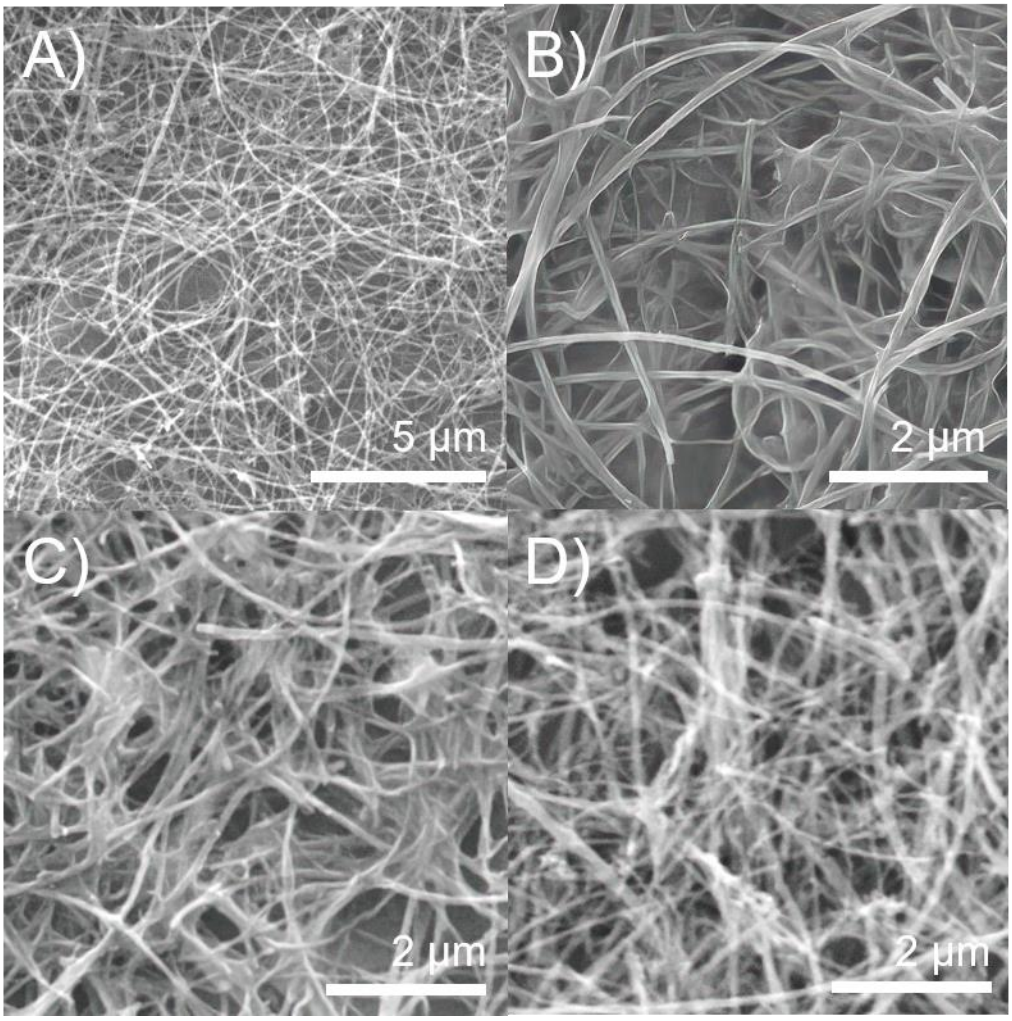

Figure S41. SEM micrographs of A) **MWCNT-2**, B) **MWCNT-*Ox*-2**, C) ***f*-MWCNT-*S*$_3$-2** y D) ***f*-MWCNT-*S*$_3$-7-2**.

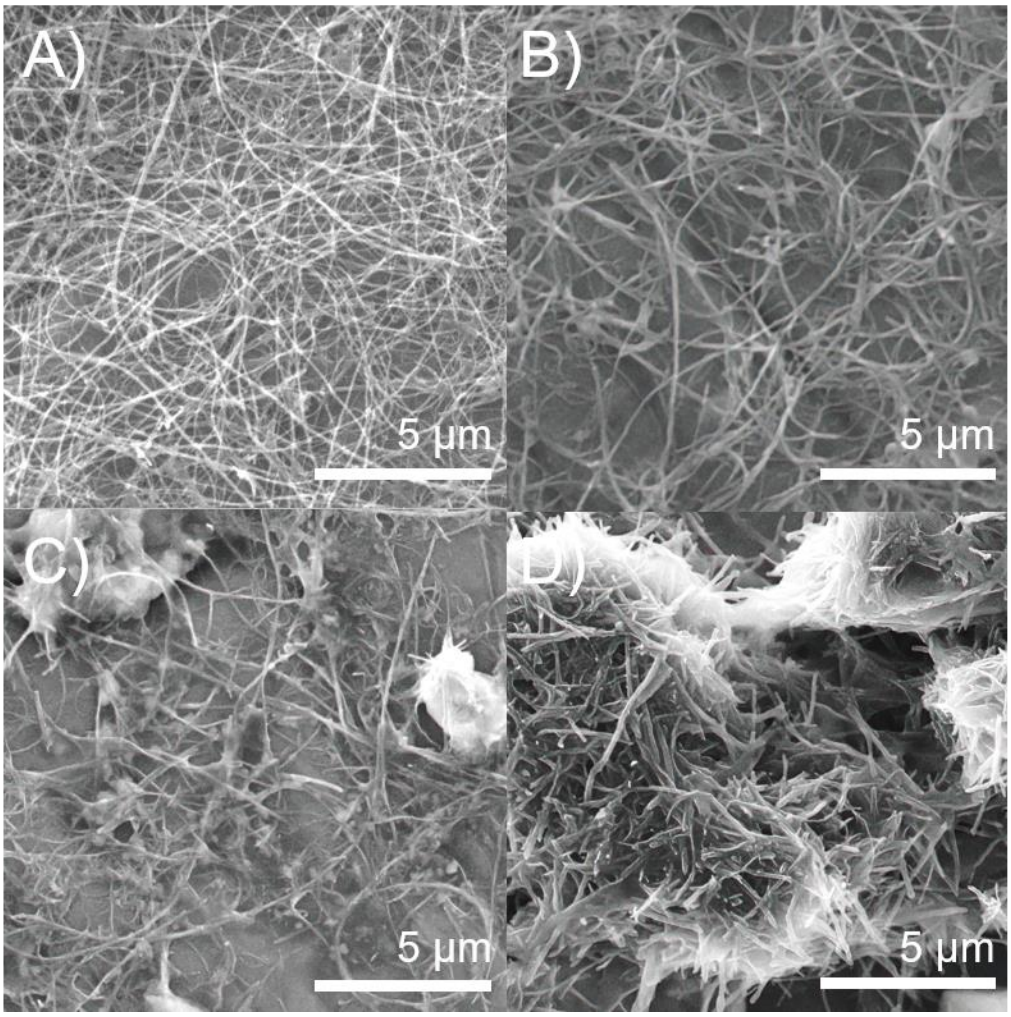

Figure S42. SEM micrographs of A) **MWCNT-1**, B) **MWCNT-*Ox*-1**, C) ***f*-MWCNT-*S*$_1$-1** y D) ***f*-MWCNT-*S*$_1$-4-1**.

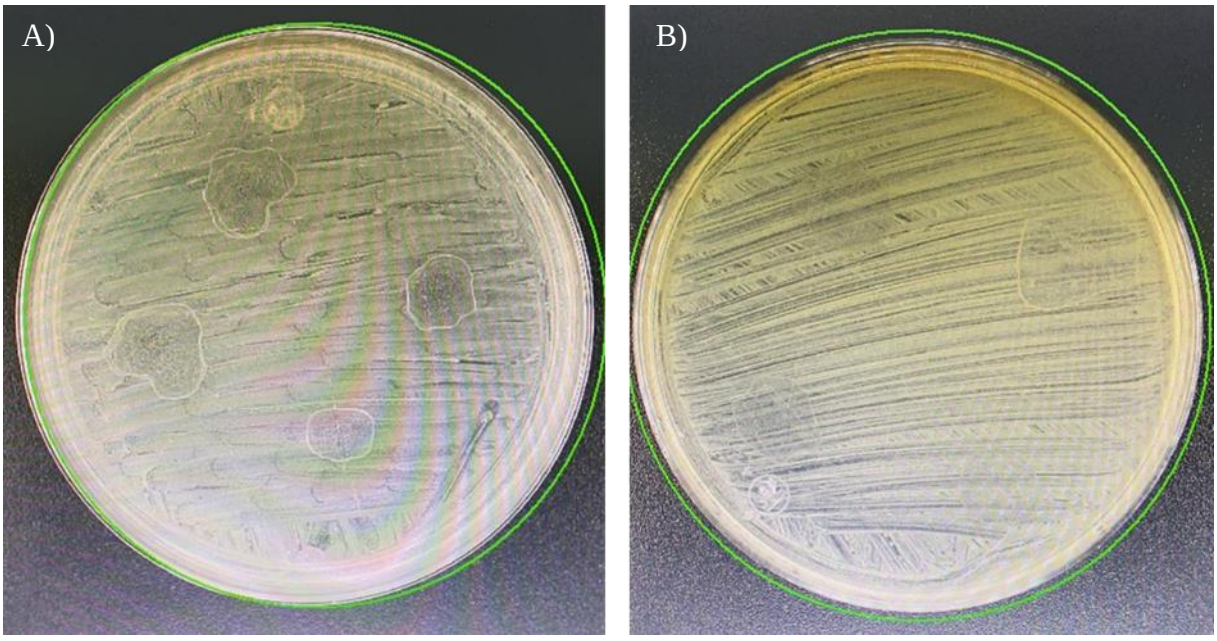

Figure S43. Radial diffusion assay for antibacterial activity of ***f*-MWCNT-*S*$_1$-4-1** with A) *S. aureus* ATCC 29213 and B) *S. aureus* clinically isolated.

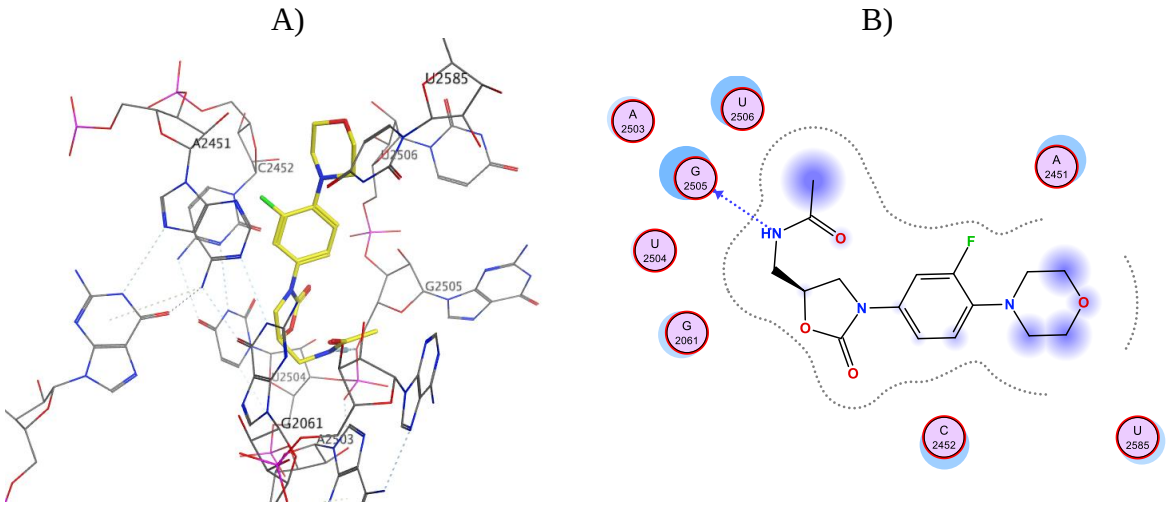

Figure S44. A) Molecular docking of Linezolid (yellow) in the PTC of *E. coli* rRNA and B) interactions map of Linezolid.

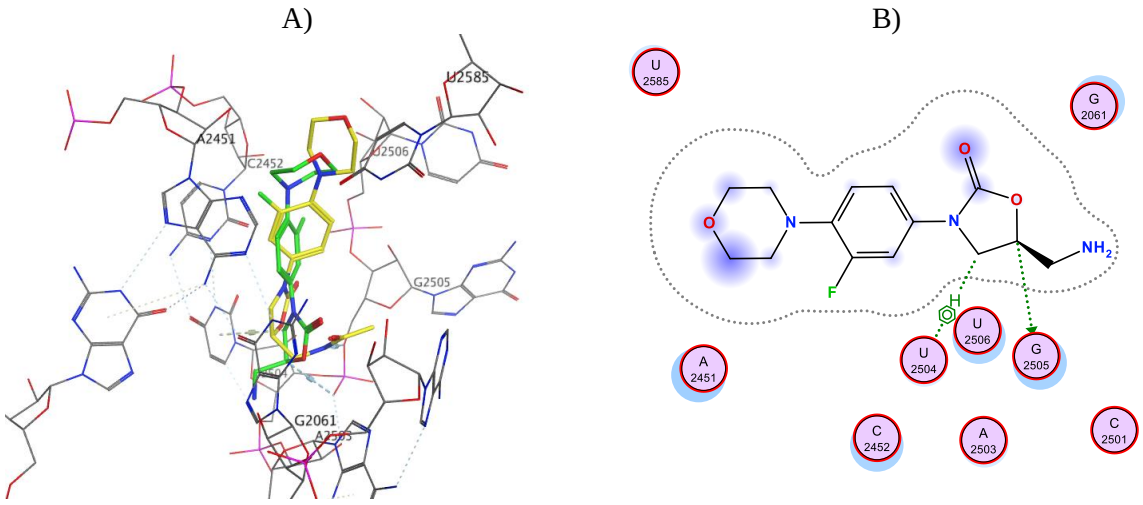

Figure S45. A) Molecular docking of **7** (pose one, yellow) and Linezolid (green) in the PTC of *E. coli* rRNA and B) interactions map of **7**.

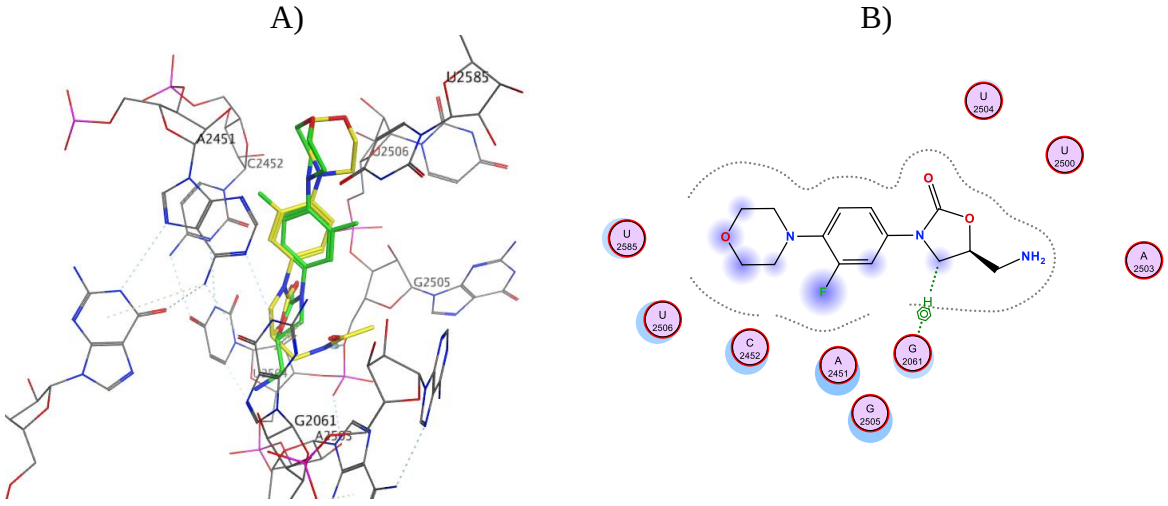

Figure S46. A) Molecular docking of **7** (pose two, yellow) and Linezolid (green) in the PTC of *E. coli* rRNA and B) interactions map of **7**.

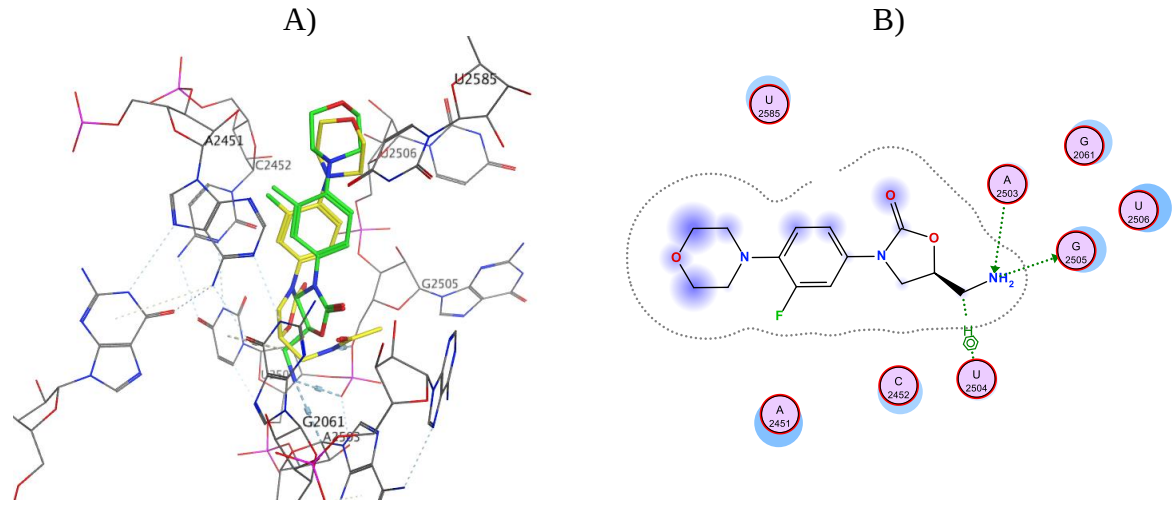

Figure S47. A) Molecular docking of **7** (pose three, yellow) and Linezolid (green) in the PTC of *E. coli* rRNA and B) interactions map of **7**.

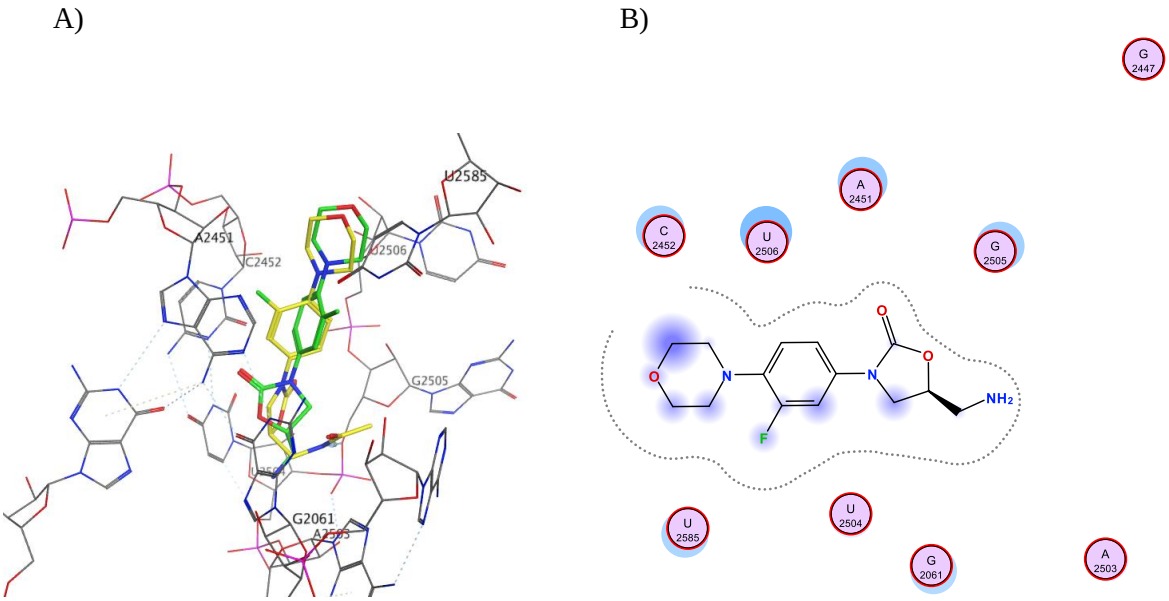

Figure S48. A) Molecular docking of **7** (pose four, yellow) and Linezolid (green) in the of *E. coli* rRNA and B) interactions map of **7**.

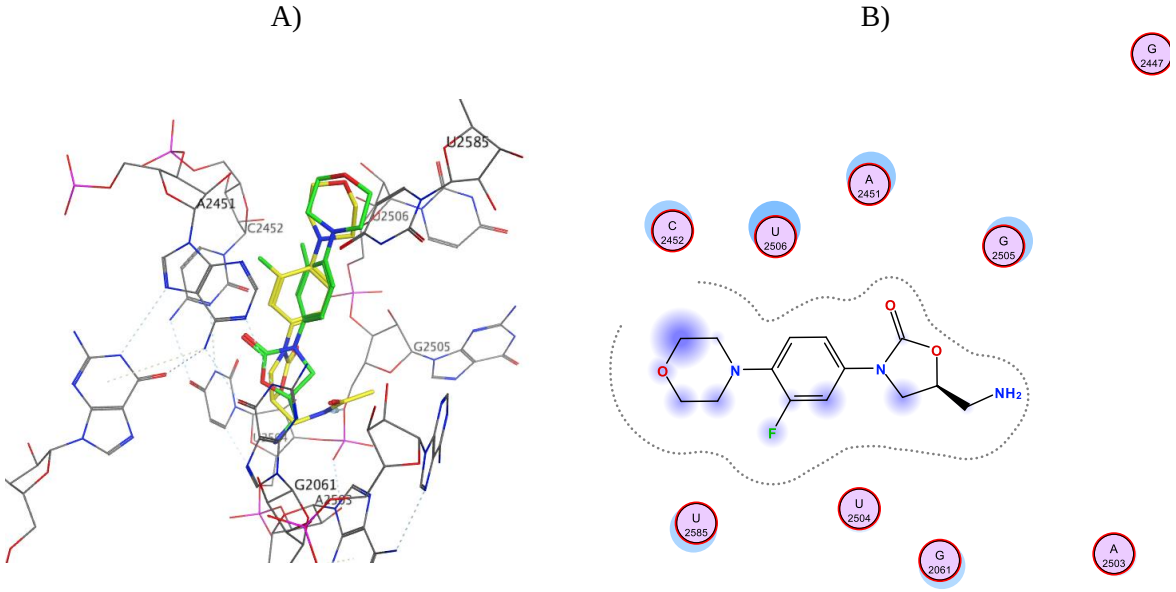

Figure S49. A) Molecular docking of **7** (pose five, yellow) and Linezolid (green) in the PTC of *E. coli* rRNA and B) interactions map of **7**.

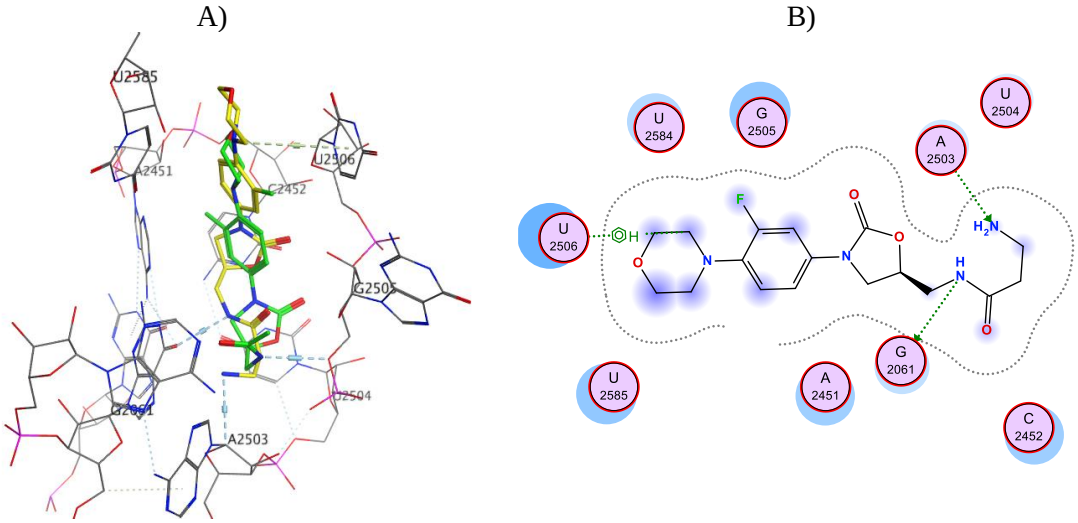

Figure S50. A) Molecular docking of ***S*$_1$-7** (yellow) and Linezolid (green) in the PTC of *E. coli* rRNA and B) interactions map of ***S*$_1$-7**.

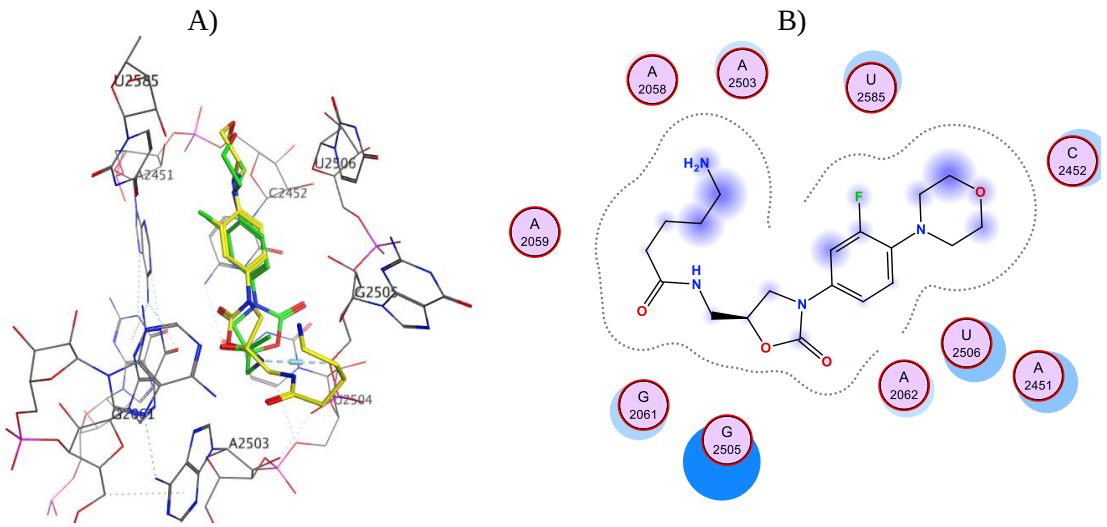

Figure S51. A) Molecular docking of ***S*$_2$-7** (yellow) and Linezolid (green) in the PTC of *E. coli* rRNA and B) interactions map of ***S*$_2$-7**.

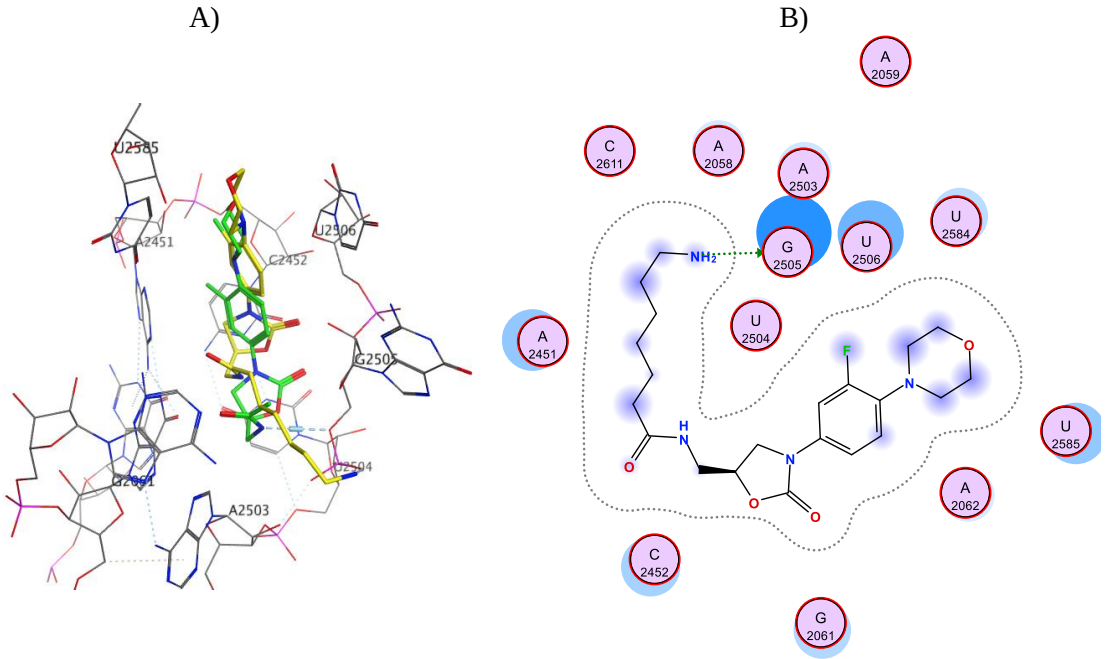

Figure S52. A) Molecular docking of ***S*$_3$-7** (yellow) and Linezolid (green) in the PTC of *E. coli* rRNA B) interactions map of ***S*$_3$-7**.

Scheme S1. Activation and functionalization of MWCNT-*Ox* with compound **7**.

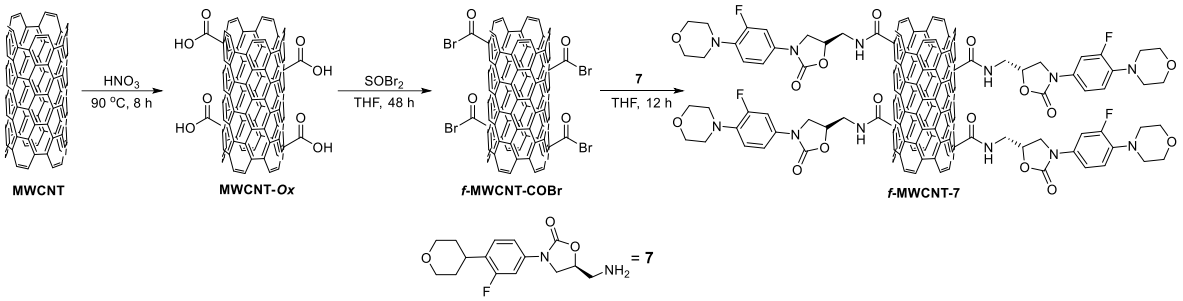

Scheme S2. Plausible mechanism for the amino-oligoethylene Linezolid analogues ***S*$_n$-7** release from MWCNTs.

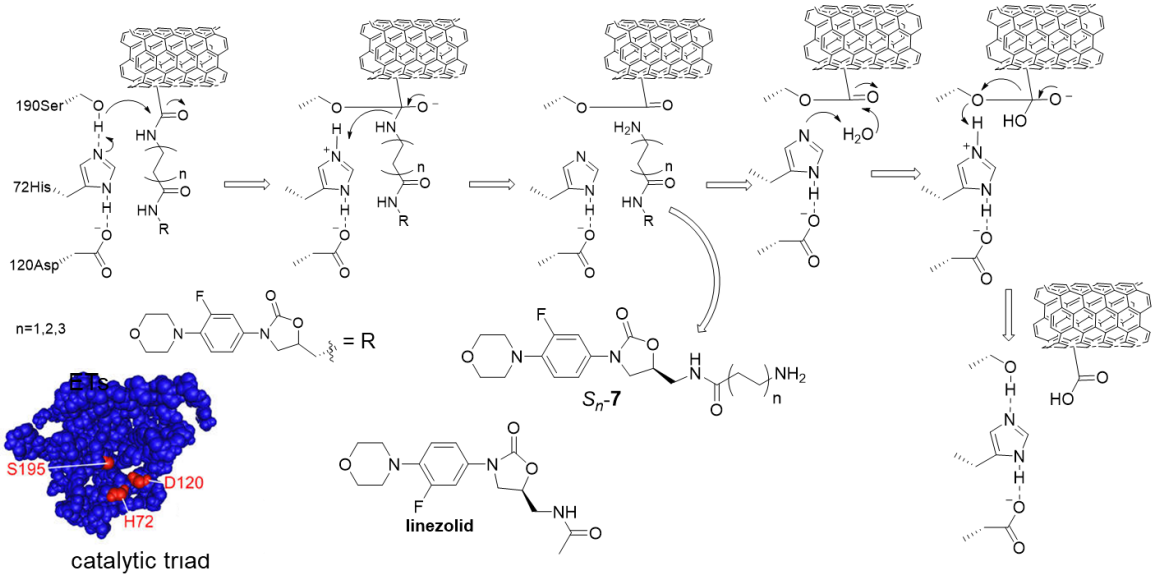

Table S1. Verification of the Lipinski rule for the compounds ***S*$_n$-7** and ***S*$_n$-7-H$^+$**.

Compounds	H-Acceptor-	H-Donor	LogP$_{(o/a)}$	Molecular Weight	TPSA
E$_1$-**7**	8	3	-0.58	366.39	97.13
E$_1$-**7**-H$^+$	8	3	-0.58	366.39	97.13
E$_2$-**7**	8	3	0.30	394.45	97.13
E$_2$-**7**-H$^+$	8	3	0.30	394.45	97.13
E$_3$-**7**	8	3	1.18	422.50	97.13
E$_3$-**7**-H$^+$	8	3	1.18	422.50	97.13
Optimum values[a,b]	<10	<5	<5	<500	<140

a. Lipinski, C. A.; Lombardo, F.; Dominy, B. W.; Feeney, P. J. Experimental and computational approaches to estimate solubility and permeability in drug discovery and development settings. Adv. Drug Deliv. Rev. 2001, 46, 3-26. doi:10.1016/S0169-409X(00)00129-0.

b. Lipinski, C. A. Lead- and drug-like compounds: the rule-of-five revolution. Drug Discovery Today: Technologies 2004, 1, 337-341. doi:10.1016/j.ddtec.2004.11.007